Glucose-dependent miR-125b is a negative regulator of β-cell function

Rebecca Cheung[§1], Grazia Pizza[§1], Pauline Chabosseau[1], Delphine Rolando[2], Alejandra Tomas[1], Thomas Burgoyne[3], Anna Salowka[1], Annabel Macklin[1], Yufei Cao[1], Marie-Sophie Nguyen-Tu [1], Piero Marchetti[4], James Shapiro[5], Lorenzo Piemonti[6], Eelco de Koning[7], Isabelle Leclerc[1], Kei Sakamoto[8], David M. Smith[9], Guy A. Rutter[1,10,11] and Aida Martinez-Sanchez*[1]

[1]Section of Cell Biology and Functional Genomics, Department of Medicine, Imperial College London, U.K.

[2]Beta Cell Genome Regulation Laboratory, Department of Medicine, Imperial College London, U.K.

[3]UCL Institute of Ophthalmology, University College London, London, U.K.

[4]Department of Clinical and Experimental Medicine, University of Pisa, Pisa, Italy.

[5]Clinical Islet Laboratory and Clinical Islet Transplant Program, University of Alberta, Edmonton, Canada.

[6]Vita-Salute San Raffaele University, Milan, Italy.

[7]Department of Medicine, Leiden University Medical Center, Leiden, The Netherlands.

[8]Novo Nordisk Foundation Center for Basic Metabolic Research, University of Copenhagen, Copenhagen, Denmark

[9]Emerging Innovations Unit, Discovery Sciences, R&D AstraZeneca, Cambridge, UK

[10]Lee Kong Chian School of Medicine, Nanyang Technological University, Singapore

[11]CR-CHUM, University of Montreal, QC, Canada

[§] Authors contributed equally

* Correspondence to: a.martinez-sanchez@imperial.ac.uk

Keywords: MiRNAs, miR-125b, islets, β-cell, insulin, hyperglycaemia, lysosomes, mitochondria, type 2 diabetes

SUMMARY

Impaired pancreatic β-cell function and insulin secretion are hallmarks of type 2 diabetes. MicroRNAs are short non-coding RNAs that silence gene expression, vital for the development and function of β-cells. MiR-125b-5p (miR-125b), a highly conserved miRNA, is abundant in β-cells, though its role in these cells is unclear. Here we show that miR-125b levels in human islets correlate with body mass index (BMI), and its expression is regulated by glucose in an AMP-activated protein kinase-dependent manner. An unbiased high-throughput screen identified multiple miR-125b targets, including the transporter of lysosomal hydrolases *M6pr* and the mitochondrial fission regulator *Mtfp1*. Inactivation of miR-125b in human β-cells shortened mitochondria and enhanced glucose-stimulated insulin secretion, whilst mice over-expressing miR-125b selectively in β-cells were glucose intolerant. β-cells from these animals contained enlarged lysosomal structures and showed reduced insulin content and secretion. Thus, we identify miR125b as a glucose-controlled regulator of organelle dynamics that modulates insulin secretion.

Highlights

- Islet miR-125b correlates with BMI and is regulated by glucose via AMP-activated protein kinase in β-cells
- miR-125b targets dozens of genes including several involved in the regulation of mitochondrial (*Mtfp1*) and lysosomal (*M6pr*) morphology or function
- Deletion of miR-125b results in shorter mitochondria and improves glucose stimulated insulin secretion (GSIS)
- Selective overexpression of miR125b in β-cells causes the appearance of enlarged lysosomes, reduced GSIS and insulin content, loss of β-cell identity and impaired insulin secretion and glucose tolerance *in vivo*

MAIN

INTRODUCTION

Pancreatic β-cells are essential regulators of glucose homeostasis, secreting insulin in response to post-prandial increases in circulating levels of the sugar[1]. Whereas an auto-immune-mediated loss of β-cell mass characterizes type 1 diabetes (T1D), type 2 diabetes (T2D) usually results from the failure of β-cells to secrete sufficient insulin to compensate for peripheral insulin resistance. Changes in β-cell function and identity[2], alongside more limited decreases in mass[3], all contribute to disease development[4]. Whereas glucose metabolism is an important positive regulator of β-cell function, chronic hyperglycaemia has a negative effect on β-cell function and survival, further exacerbating the disease[5]

MicroRNAs (miRNAs) are tiny (~21 ntd (nucleotide)) non-coding RNAs that silence gene expression post-transcriptionally. Since their discovery almost two decades ago, miRNAs have been widely demonstrated to play important regulatory roles in most biological processes and in many diseases[6]. Even though it is now well established that miRNAs are essential for endocrine cell development and function[7] and that β-cells contain hundreds of different miRNAs, the function of only a few of these has been studied in detail.

MiR-125b (miR-125b-5p) is a highly conserved miRNA widely studied in the context of tumorigenesis and immunology and an important regulator of cellular proliferation, differentiation and apoptosis[8]. We have previously shown that miR-125b expression increases in islets after β-cell specific deletion of the AMP-activated protein kinase (AMPK) catalytic subunits α1 and α2 (βAMPKdKO)[9], suggesting that AMPK may act as a negative regulator of miR-125b expression. AMPK is an evolutionarily-conserved protein kinase whose activity is suppressed acutely in the β-cell by high glucose[10], and lowered in islets from subjects with T2D diabetes[11, 12].

The above observations have led us to hypothesize that inhibition of AMPK in response to high glucose would result in islet miR-125b up-regulation which may mediate some of the

deleterious effects of hyperglycaemia in β-cells. We aimed to test this hypothesis here and to explore the possible implications for disease pathogenesis. We show that high glucose increases islet miR-125b expression and that miR-125b has an important negative effect in β-cell function both *in vitro* and *in vivo* by targeting genes involved in regulating lysosomal and mitochondrial function.

RESULTS

Glucose stimulates miR-125b expression via AMPK repression

In order to determine whether glucose regulates miR-125b expression in islets, we measured miR-125b in mouse and human islets cultured at increasing glucose concentrations. As shown in Figure 1a, miR-125b expression was significantly increased after culture for 48h at high (11-25mM) vs low (3.5-5.5 mM) glucose concentrations. Consistent with the possible *in vivo* relevance of these findings, expression of miR-125b in human islets was positively correlated with the body mass index (BMI) of (non-diabetic) donors (Figure 1b). The latter parameter is associated with increased blood glucose[13]. No association was found between miR-125b expression in islets and the age or sex of the donors (Supp Figure 1).

Islets from βAMPKdKO mice displayed significantly higher miR-125b levels than controls when cultured at a low (5.5mM) glucose concentration (Figure 1c) whereas miR-125b expression remained unchanged when islets were cultured at high glucose (25mM). To determine whether this glucose/AMPK-dependent regulation of miR-125b also occurred *in vivo*, we fed control, βAMPKdKO or βLKB1KO (mice with a β-cell specific deletion of the AMPK-upstream kinase Liver kinase B1, LKB1/STK11[14]) animals a ketogenic (low sugar) diet. In agreement with our previously published data[9], βAMPKdKO islets displayed higher levels of miR-125b than controls (Figure 1d) and, as expected, the same islet miR-125b up-regulation was observed in βLKB1KO islets (Figure 1d). As demonstrated in figure 1d, feeding a low-sugar diet for 28 days resulted in a significant decrease in islet miR-125b in control animals. Nevertheless, miR-125b levels remained identical in islets from βAMPKdKO and

βLKB1KO mice fed a chow or a ketogenic diet (Figure 1d). Moreover, culture of human islets with the selective AMPK activators C13 and 991[9] caused a small but significant reduction in miR-125b expression (Figure 1e). Taken together, these results suggest that high glucose stimulates miR-125b expression in both mouse and human islets, *in vivo* and *in vitro*, by inhibiting AMPK.

MiRNAs are transcribed as longer primary transcripts (pri-miRNAs) that are first processed in the nucleus into ~70 ntd hairpins (pre-miRNAs) and later, within the cytoplasm, into mature (~21 ntd) miRNAs[15]. Consequently, mature miRNA expression can be controlled at different levels, including transcription, processing and stability. MiR-125b is encoded by two independent *loci*, *MIR125B-1* and *MIR125B-2* in humans and mice, located on Chr11 and Chr21 (humans) and Chr9 and Chr16 (mice), respectively. Several (2-3) transcriptional initiation (start) sites (TSS) as close as ~2KB and as far as ~200KB upstream the annotated pre-miR-125b have previously been identified[8 16]. RT-qPCR of pri-miR-125b-1/2 demonstrated that, as for (mature) miR-125b, βAMPKdKO islets expressed significantly higher levels of pri-miR-125b-1 than controls (Figure 1f), suggesting that AMPK inhibits the production of miR-125b precursors and therefore transcription. Of note, we were not able to detect pri-miR-125b-2, indicating low transcription rate and/or fast processing of this precursor.

Ottaviani and co-workers[17] have recently demonstrated that miR-125b is induced by TGF-β *via* Smad2/3 activation of the *MIR125B-1* locus in pancreatic ductal adenocarcinoma cells (PDAC). Interestingly, Smad2/3 ChIP-seq in mouse islets showed binding to an annotated miR-125b TSS (Supp Figure 2) located in a chromatin region with increased accessibility in βLKB1KO islets (Cebola et al. *in preparation*, Supp Fig 2). Nevertheless, contrary to what we expected, transfection of MIN6 cells with siRNAs against Smad3 siRNAs resulted in a small increase in miR-125b, whereas no effect was observed with Smad2 siRNAs (Supp Figure 3), suggesting that Smad2/3 are not transcriptional activators of miR-125b in MIN6 cells.

MiR-125b regulates insulin secretion in β-cell lines

The most important characteristic of the β-cell is its capacity to respond to high levels of circulating glucose by secreting insulin, a process that is tightly regulated[1]. We thus set to determine whether miR-125b plays a role in this process by short-term (48h) over-expression of miR-125b in the mouse insulinoma cell line MIN6. Glucose-stimulated insulin secretion from MIN6 cells transfected with miR-125b mimics was 30% lower (p=0.1) *vs* control transfected cells and, more strikingly, these cells contained 40% less insulin (p=0.03) (Figure 2a).

To explore whether miR-125b regulated insulin secretion from human β-cells and under physiological conditions, we next generated human EndoCβ-H1 cells[18] with miR-125b loss-of-function using CRISPR-Cas9. EndoCβ-H1 cells were infected with a lentiviral vector expressing one of two different pairs of gRNAs targeting each *MIR125B* locus *(MIR125B-1 and MIR125B-2)* and a rat *Insulin* promoter-driven hSpCas9 expression cassette (Supp Figure 4a). Independently, both gRNA pairs targeting the *MIR125B-2* locus (*MIR125B2-KO1* and *MIR125B2-KO2*) resulted in cell populations with strongly reduced (~80%) levels of mature miR-125b while gRNAs targeting *MIR125B-1* resulted in a marginal reduction of the miRNA (Supp Figure 4b) and cells infected with lentivirus bearing gRNAs against both loci showed a more limited (~40-60%) decrease in miR-125b expression (Supp Figure 4c). These results indicate that most mature miR-125b is transcribed from *MIR125B-2* in EndoCβ-H1 cells. Consequently, we used our *MIR125B-2* CRISPR-cells (KO1, hereafter EndoCβH1-MIR125B2-KO) for further characterization. Expression in EndoCβH1-MIR125B2-KO cells of the other member of the miR-125 family, miR-125a and of miR-99a, annotated in the same genomic cluster as *MIR125B-2* (Supp Figure 4b) did not differ from control (Cas9-expressing) cells. As anticipated, EndoCβH1-MIR125B2-KO cells secreted more insulin in response to high glucose than controls, although no differences were detected in insulin content (Figure 2d).

High-through identification of miR-125b target genes

MiRNAs can target hundreds of genes simultaneously and in a cell type-specific manner[19] providing the capacity to tightly regulate biological processes. To further explore the genes

and molecular pathways regulated by miR-125b, as well as its mechanism of action, we sought to explore the impact of the miRNA on β-cell gene expression and to identify direct targets in a high throughput manner. MiRNAs guide the miRNA-induced silencing complex (miRISC), including an ARGONAUTE protein to the target mRNAs *via* partial sequence complementarity. Thus, an mRNA that is actively repressed by miRNAs will be bound to miRISC. MiRISC's action will result in target mRNA destabilization[20] and/or inhibition of target mRNA translation without observable changes in transcript levels. Thus, we used an experimental approach that combined overexpression of miR-125b in MIN6 cells, immunoprecipitation of miRISC/target mRNAs using an antibody against AGO2 and high-throughput sequencing and differential analysis of cellular total and immunoprecipitated RNAs[17, 21] (Figure 3a). As a consequence of miR-125b overexpression, we expected miR-125b targets to be reduced or unchanged (if repression occurs exclusively at the level of translation) in the total mRNA (T-RNA, Sup Table 1) fraction and increased in the precipitated (RIP-RNA, Supp Table 1) fraction. Thus, for miR-125b direct targets we expect a RIP-RNA to T-RNA ratio > 1 following miR-125b overexpression. In order to validate our approach we sorted all detected genes according to RIP-RNA/T-RNA ratio (Supp Table 1) and performed unbiased word enrichment analysis using cWords[22]. As anticipated, cWords found a significant enrichment of miR-125b seed-matching sequences in highly ranked (high RIP-RNA/T-RNA ratio) genes (Figure 3b). Importantly, enrichment on seed-complementary sequences was found in both the 3' non-translated (3'UTR) and coding (CDS) sequences of highly ranked genes, though a higher Z-score (>20) was obtained for 3'UTRs (Figure 3b). This suggests that miR-125b-mRNA target interactions occur both *via* the 3'UTR and CDS. 182 mRNAs were enriched in miRISC following miR-125b overexpression with an RIP-RNA/T-RNA > 1.5 (Figure 3c, Table 1). Out of these, only 60 were significantly down-regulated at the mRNA level following miR-125b overexpression (Table 1, padj < 0.1) and 87 contained predicted binding sites in their 3'UTRs according to TargetScan (Table 1).

We decided to further validate the six targets (*Taz*, *M6pr*, *Tor2a*, *Mtfp1*, *Tnks1bp1* and *Gnpat*) with the highest RIP-RNA/T-RNA ratios using luciferase-based assays[23]. Whereas *Taz*, *M6pr*, *Tor2a* and *Mtfp1* contain predicted binding sites in their 3'UTRs, *Tnks1bp1* and *Gnpat* contained sequences complementary to miR-125b in their CDS (RNAhybrid, mfe: 32.5 and 24.3 kca/mol, respectively). Therefore, we generated constructs containing the 3'UTR of *Taz*, *M6pr*, *Tor2a* and *Mtfp1* and the CDS of *Tnks1bp1* and *Gnpat* under the *Firefly* open reading frame (ORF) in the bicistronic plasmid pMiRGlo which also encodes for *Renilla* luciferase. As expected, co-transfection of miR-125b mimics reduced *Firefly*/*Renilla* activity in cells transfected with constructs containing the *Taz*, *M6pr*, *Tor2a* and *Mtfp1* 3'UTRs and *Gnpat* CDS, demonstrating that miR-125b silence gene expression through those sequences (Figure 4a). We failed to validate miR-125b action through *Tnks1bp1* CDS, since cells transfected with this construct displayed the same *Firefly*/*Renilla* activity in the presence of miR-125b or control mimics, perhaps due to the location of the binding site downstream the luciferase CDS and not within the CDS itself[24]. As expected, miR-125b mimics strongly reduced *Firefly*/*Renilla* activity of a reporter containing three perfectly complementary sequences to miR-125b and did not affect *Firefly*/*Renilla* activity of the empty vector or in the presence of the 3'UTR of *Gnpat* which doesn't contain predicted miR-125b binding sites.

MiR-125b targets genes encoding mitochondrial and lysosomal proteins

To identify biological pathways and functions regulated by miR-125b we submitted the list of genes dysregulated at the RNA level (T-RNA, 306 genes down-regulated and 317 up-regulated padj < 0.1, Supp Table 1) as well as those genes identified as miR-125b direct targets with a RIP/T-RNA > 1.5 (Table 1) to a Database for Annotation, Visualization and Integrated Discovery, DAVID[25]. We applied DAVID's newly-added clustering tool to group similar annotations from UniProtein Keywords (Functional category), Biological Processes, Cellular Compartments and Molecular Functions (Gene Ontology terms, GO) and Kyoto Encyclopedia of Genes and Genomes (KEGGs) Pathways. Functional annotations with high enrichment scores included mitochondrion, tricarboxylate (TCA) cycle, sterol biosynthesis,

protein transport, Golgi apparatus and endosome (Figure 4b, Supp Table 2), all closely associated to the capacity of the β-cells to produce and secrete insulin in response to glucose.

The lysosomal/Golgi-associated *M6pr* (Manose-6-phosphate receptor-cation dependent, M6PR-CD) is one of the genes at the top of our list of newly-identified miR-125b targets in MIN6 cells. M6PR-CD controls trafficking of lysosomal hydrolases from the Golgi via endosomes[26] and thus may influence protein turnover and lysosomal function. Luciferase assays further confirmed the interaction of miR-125b *via* a predicted conserved miR-125b binding site in its 3'UTR (Figure 5a). Even though we were not able to detect mouse M6PR protein, Western-(Immuno) blot of EndoCβ-H1 cells overexpressing miR-125b and EndoCβH1-MIR125B2-KO cells showed a strong down- and up-regulation in M6PR protein, respectively (Figure 5b) without significant changes at the mRNA level (Figure 5c and Supp Table 3). These results confirm that miR-125b targets M6PR to repress protein production in both mouse and human β-cells.

We next hypothesized that miR-125b overexpression might lead to M6PR downregulation, and consequently to a defect in lysosomal hydrolases. This may in turn lead to an accumulation of lysosomal structures with non-digested organelles and proteins. To test our hypothesis, we performed electron microscopy (EM) on MIN6 cells transfected with control or miR-125b mimics. Interestingly, miR-125b overexpressing cells displayed an accumulation of aberrant lysosomal structures with enlarged lysosomes (Figure 5d).

As mentioned above, GO of genes dysregulated upon miR-125b overexpression also revealed a significant over-representation of genes involved in mitochondrial function and oxidoreductase activity (Supp Table 2, Figure 4b), including one of the top miR-125b direct targets, mitochondrial fission process 1 (*Mtfp1*, also known as MTP18). As shown in Figure 6a, Mtfp1 3'UTR cloned downstream Firefly ORF mediated *Firefly/Renilla* luciferase reduction in the presence of miR-125b mimics. Importantly, mutation of the predicted and conserved miR-125b binding site de-repressed luciferase activity (Figure 6a), demonstrating that the direct interaction of miR-125b with this binding site is responsible for the repression.

MTFP1 has previously been implicated in mitochondrial fission and apoptosis in mammalian cells[27]. Mitochondria undergo constant fusion and fission processes that ensure quality control and adequate function[28]. To explore a possible role for miR-125b in controlling mitochondrial morphology, we stained MIN6 cells transfected with control or miR-125b mimics with a mitochondria-targeted green fluorescent probe (Mitotracker green). MIN6 cells overexpressing miR-125b contained the same number and overall mitochondrial area, though their mitochondria were slightly more elongated and less circular (Figure 6b). In contrast, mitotracker green staining of EndoCβH1-*MIR125B2-KO* cells revealed a marked reduction in mitochondrial area and a higher number of mitochondria with a smaller perimeter, and which were also less elongated and more circular (Figure 6c). These findings suggest that whereas endogenous miR125b levels are sufficient to exert maximal effects on mitochondrial structure, relief from miR125-mediated repression of the fission machinery leads to disruption of the tubule-vesicular network.

Further emphasizing the importance of miR-125b for mitochondrial homeostasis, GO analysis following RNAseq of EndoCβH1-MIR125B2-KO confirmed a strong enrichment in dysregulated genes associated with mitochondrial function (Figure 6d, Supp Table 4). Of note, whilst we identified 609 and 81 genes up- and down-regulated, respectively (Sup Table 3, padj<0.1) in EndoCβH1-MIR125B2-KO, miRNA binding site enrichment analysis of up-regulated genes using cWords or Mienturnet[29] failed to identify an enrichment in genes with predicted miR-125b binding sites (p=0.2), with only 30 genes containing conserved predicted miR-125b binding sites (Supp Table 3) and an additional 108 containing at least one non-conserved binding site (data not-shown). Even though we were we unable to detect MTFP1 protein in MIN6 or EndoCβH1 cells with two different commercial antibodies tested, up-regulation of *MTFP1* mRNA was confirmed by the RNA-seq data in EndoCβH1-MIR125B2-KO cells (MTFP1, 1.5 fold, p-value: 0.006, padj 0.1, Sup Table 4).

Taken together, these data indicate that long-term reduction of miR-125b expression in human EndoCβ-H1 cells has a strong direct and indirect effect in the expression of genes involved in mitochondrial homeostasis which may underlie the observed improvement in insulin secretion.

MiR-125b overexpression in β-cells impairs glucose tolerance *in vivo*

Given the powerful effect of miR-125b manipulation on β-cell gene expression and function *in vitro*, we decided to study the role of miR-125b *in vivo* by generating a mouse with β-cell specific, inducible overexpression of miR-125b using the Tet-ON system[30]. Mice bearing a transgene expressing miR-125b under the control of an rtTA-inducible rat insulin promoter (MIR125B-Tg: RIP7-rtTA$^{+/-}$, MIR125B Tg$^{+/-}$) and controls (Control: RIP7-rtTA$^{+/-}$) were continuously administered doxycycline (from parental mating) in the drinking water and were born at the expected mendelian ratios (50% each). RT-qPCR in islets isolated from 6-10 week old MIR125B-Tg animals revealed ~60-fold more mature miR-125b in comparison to Control mice (Figure 7a). On the other hand, miR-125b levels remained unchanged in the hypothalamus of MIR125B-Tg animals, a potential site for activity of the RIP2 promoter [31] (Supp Figure 5a).

MIR125B-Tg mice showed indistinguishable weight gain than controls as measured between 5-10 weeks of age (Supp Figure 5b). In contrast, random-fed glycaemia was significantly higher in MIR-125B-Tg when measured at 5 and 9 weeks of age, in both male and females (Figure 7b). Consistently, both male and female MIR125B-Tg mice were highly glucose intolerant at both 6 and 10 weeks of age (Figure 7c/d), though fasting glycaemia was unaffected. No changes in glucose tolerance were observed in animals bearing the transgene in the absence of rtTA (-rtTA Control: RIP7-rtTA$^{-/-}$, MIR125B OE$^{+/-}$, Supp Figure 5c), demonstrating that the defects observed were not due to an off-target genomic event resulting from transgene integration. Blood glucose levels were efficiently reduced by administration of exogenous insulin, as measured by intraperitoneal insulin tolerance test in male and female MIR125B-Tg and Control mice at 7 weeks of age, excluding insulin insensitivity as a major player in the glucose intolerance observed in MIR125B-Tg animals (Supp Figure 5d).

Moreover, MIR125B-Tg mice failed to secrete insulin in response to an intraperitoneal injection of glucose (Figure 7e) suggesting impaired β-cell secretory function. β-cell mass and β- to α-cell ratio remained unchanged in the transgenic animals (Figure 7f). Accordingly, no differences were observed in β-cell proliferation or apoptosis (Supp Figure 5e/f).

Taken together, these data suggest that increased miR-125b in the β-cell results in hyperglycaemia and glucose intolerance due to impaired β-cell secretory function but not β-cell mass.

MiR-125b transgenic islets contain and secrete less insulin

To further explore a cell autonomous defect in insulin secretion, we measured glucose-stimulated insulin secretion (GSIS) in islets isolated from control and MIR125B-Tg mice. Islets isolated from MIR125B-Tg mice showed a strong reduction in insulin secretion in response to glucose or depolarisation by KCl (Figure 8a). Consistent with our previous data in MIN6 cells, MIR125B-Tg islets contained less intracellular insulin (Figure 8b), as further confirmed by Western blot (Figure 8c). The latter revealed lower levels of both intracellular pro-insulin and insulin. These data indicate a reduced capacity of miR-125b-overexpressing β-cells to produce and secrete insulin, a defect likely to underlie glucose intolerance in the transgenic mice.

Upon entry in the β-cell, glucose is rapidly metabolized by mitochondria which causes a sharp increase in intracellular ATP/ADP ratio which, in turn, closes the ATP-sensitive K^+ (K_{ATP}) channels leading to plasma membrane depolarization and Ca^{2+} influx into the cytosol to trigger insulin exocytosis[1]. The fact that secretory responses to both high glucose and KCl were impaired in MIR125B-Tg islets suggested a defect downstream of glucose metabolism. Interestingly, the glucose-mediated ATP/ADP rise was identical in MIR125B-Tg and Control isolated islets (Figure 8d), and basal ATP/ADP ratio was slightly but not significantly higher in transgenic islets *versus* control islets (Figure 8e). In contrast, MIR125B-Tg islets showed a strong reduction in glucose-induced changes in intracellular Ca^{2+} (Figure 8f). KCl-induced rises

in free Ca^{2+} were, on the other hand, similar between MIR-125B-Tg and Control islets, suggesting that MIR125B-Tg β-cells contained functional voltage-gated calcium channels (Figure 8f).

To assess the rate and kinetics of vesicle exocytosis we used total internal reflection of fluorescence (TIRF) imaging to image neuropeptide Y (NPY)-Venus-expressing vesicles near the plasma membrane[32]. As shown in figure 8g, the kinetics of individual fusion events were similar in cells from MIR125B-Tg or Control islets, indicating that vesicle fusion itself was not affected by miR-125b overexpression.

Enlarged lysosomes/autophagolysosomes are abundant in miR-125b transgenic islets

Our previous experiments in MIN6 and EndoCβ-H1 cells pointed to miR-125b as a regulator of mitochondrial and lysosomal function, which could contribute to defective insulin secretion. To determine whether a similar mechanism was involved in primary β-cells, we stained transgenic and control islets with mitotracker- and lysotracker-green to visualize mitochondria and lysosomes, respectively. In contrast to our observations in cell lines, but consistent with an efficient capacity to generate ATP in response to glucose, mitochondrial area and morphology (i.e. circularity) were comparable in MIR125B-Tg and Control (Figure 9a), as well as the levels of mitochondrial DNA (mtDNA, Figure 9b). Even though no significant differences were found in the total number of lysosomes or in the lysosomal area in MIR125B-OE islets as measured by lysotracker imaging (Supp Figure 5g), transmission electron microscopy (TEM) analysis identified the presence of enlarged lysosomes and autophagosomes in the transgenic islets which were rarely found in Control samples (Figure 9c,d). TEM also revealed a sharp reduction in the mature/immature insulin granule ratio in MIR125B-Tg islets, with significantly fewer mature (dense core) and more immature (with defective crystalization) insulin granules (Figure 9e). Importantly, fewer secretory granules were present within 200nm of the plasma membrane in MIR125B-Tg than in control islets (Figure 9e).

β-cell identity is altered in MIR125b-Tg islets

To shed more light into the molecular mechanisms underlying the secretory defects of miR-125B-Tg islets, we performed RNA-seq on MIR125B-Tg and Control islets from 6 week old mice. 320 genes were significantly (padj <0.1) down-regulated and 398 up-regulated, respectively (Supp Table 5). Mienturnet identified an enrichment of predicted miR-125b binding sites within the down-regulated genes (p-value <0.001, FDR=0.02), though only 31 genes contained predicted conserved targets (Supp Table 5) and 85 poorly conserved targets (data not shown), suggesting that many of the effects observed following β-cell specific, long-term overexpression of this miRNA, are indirect.

Several important β-cell identity genes such as *Ucn3, Pdx1, NeuroD1, Nkx2.2, Slc2a2* and *Nkx6.1* were significantly reduced in MIR125B-Tg islets and, accordingly, GO analysis of downregulated genes identified a strong enrichment within pathways and processes associated with mature β-cell function. These included regulation of insulin secretion, response to glucose, glucose homeostasis and endocrine pancreas development (Supp Table 6, Figure 10a, b). Further supporting a loss of β-cell identity, up-regulated genes were significantly associated with neuronal features (nervous system development, axon, neuronal cell body, etc. Supp Table 6, Figure 10a). Moreover, we observed an upregulation of many glycoprotein genes (Supp Table 6, Figure 10a) and of genes associated with cellular and focal adhesion, migration, signalling pathways and voltage-gated and potassium channels. Golgi-associated genes were both up and down-regulated (Supp Table 6, Figure 10a).

MiR-125b alters gene expression in human islets

To further explore the relevance of miR-125b in human β-cells, we performed RNA-seq in dissociated human islets from three different donors infected with an adenovirus expressing miR-125b, achieving a ~3 fold increase in miR-125b levels (Supp Figure 6a). Principal component analysis (PCA) showed that most of the variation was due to the donor origin of the islets (Supp Figure 6b) and, thus this experiment was underpowered due to the high variability observed in gene expression between individuals (power achieved is ~20% to detect a 2x Fold change with p<0.01, as calculated using Scotty[33]). Thus, we only detected four

dysregulated genes with a padj value <0.1 although the expression of hundreds of genes tent to be altered (p-value <0.05, Sup Table 7). Gene Set Enrichment analysis of all the detected genes ranked by fold change in gene expression identified a significant enrichment in several biological pathways (Figure 10c, Sup Table 8) notably including lysosomal (p<0.0001, FDR=0.07) and calcium signalling (p<0.0001, FDR=0.06) amongst the down- and up-regulated pathways.

DISCUSSION

Despite being highly expressed in β-cells[34], the function and mechanism of action of miR-125b in these cells have remained elusive until now. Here, we show that hyperglycaemia induces islet miR-125b expression and that elevated expression of this miRNA in β-cells impairs secretory function *in vitro* and *in vivo*.

β-cell dysfunction is a key element in the development of diabetes although the molecular and cellular nature of these changes are contested and are likely to be multifactorial[35]. Hyperglycaemia impairs β-cell function and insulin secretion by several mechanisms including loss of cellular identity, impaired glucose metabolism and increased apoptosis[36]. Three independent studies identified higher levels of circulating miR-125b in association with higher HbA1c in T1D[37], T2D[38] and in patients with gestational diabetes (GDM)[39], though the levels of miR-125 in pancreatic islets or other metabolic tissues were not assessed. Even though the human islets used in this study originated from different sources and HbA1c data was not usually available, we were able to observe a significant correlation between islet miR-125b levels and donor BMI, which often associates itself with HbA1c [13]. More importantly, glucose-induced miR-125b expression in both mouse and human islets *in vitro* and feeding mice a low-sugar (ketogenic) diet strongly reduced islet miR-125b levels.

Our studies, which used both chemical activation and genetic ablation of AMPK, demonstrate that AMPK mediates glucose regulation of mouse and human islet miR-125b, possibly at the transcriptional level. Nevertheless, the molecular players responsible of miR-125b

transcriptional regulation remain to be identified and our results do not discard post-transcriptional mechanisms, such as pri-/pre-miRNA processing or mature miR-125b stability, as additional contributors to glucose/AMPK-mediated regulation of miR-125b expression.

Here, we have generated a transgenic model capable of β-cell selective overexpression of miR-125b. These animals were hyperglycaemic and strongly glucose intolerant and presented a drastic reduction in circulating insulin following a glucose challenge. In a paper published during the preparation of this manuscript, Wei and colleagues[40] showed that whole-body *MIR125B-2* knockout mice on a high-fat diet, but not on a normal diet, develop insulin resistance and glucose intolerance possibly due to the accumulation of epididymal and inguinal white fat. Consequently, these authors suggest the systemic delivery of miR-125b mimics to intervene obesity-related diseases. Nevertheless, insulin secretion or an effect in other metabolic organs was not assessed in these mice, nor were the molecular mechanism(s) underlying the accumulation of adipocytes explored. Additionally, other studies contest whether miR-125b overexpression might be beneficial for adipocyte function [41] [42] [42]. Consistent with this view, systemic, non-targeted injection of miR-125b *in vivo* led to random-fed hyperglycaemia and glucose and insulin intolerance in mice[43].

The present study provides compelling evidence of a role for miR-125b in controlling insulin secretion, and strongly indicates that non-targeted administration of miR-125b mimics may reach the islet and lead to defective β-cell function and worsen diabetes. The findings suggest two main causes for the glucose intolerance observed in MIR125B-Tg mice: strong defects in insulin secretion in response to glucose and reduced insulin content of the transgenic islets.

Unlike ATP, cytosolic Ca^{2+} increases following glucose stimulation were substantially lower in MIR125b-Tg islets though, paradoxically, similar levels of Ca^{2+} were observed upon membrane depolarization with KCl, even though KCl-stimulated insulin secretion was also strongly impaired. These results point towards defects at different levels on the secretory pathway, as supported by the striking changes in gene expression. First, several K_{ATP}-independent amplification pathways have been extensively demonstrated to play important

roles in GSIS[44]. For example, Gooding and colleagues[45] showed that glucose induces changes in purine pathway intermediates that promote exocytosis in an ATP/ADP ratio independent manner. Accordingly, inhibitors of Inosine-5'-monophosphate dehydrogenase (IMPDH), a rate-limiting enzyme for the production of guanine nucleotides impaired GSIS by reducing S-AMP levels and Sentrin-specific protease 1 (SENP1)-dependent exocytosis. Interestingly, MIR125B-Tg islets displayed a 40% reduction on *Imphd1* mRNA (padj 0.016) as well as lower levels of glutamine synthetase (GS, *GLUL*), a limiting enzyme for glutamine synthesis the inhibition of which reduced GSIS [46]. Of note, glutamine has been shown to strongly increase Ca^{2+} influx in the presence of glucose, without changes in ATP content[47]. Secondly, decreased insulin secretion following KCl-mediated membrane depolarization in the absence of reduced intracellular Ca^{2+} suggests the presence of functional voltage-dependent Ca^{2+} channels in transgenic islets and points towards defects in the final steps of exocytosis. Further supporting this idea, expression of genes encoding Ca^{2+} channels was not significantly altered in MIR125B-Tg islets. Whereas TIRF experiments revealed no changes in the kinetics of granule fusion at the plasma membrane, TEM revealed fewer granules in close proximity to the plasma membrane (< 200 nm) in MIR125B-Tg *vs* Control β-cells. Regarding the mechanism resulting in reduced granule docking, our RNAseq identified a strong reduction in granuphilin (*Sytl4* 0,58 fold, p-adj 0.002) which mediates dense core granules docking to the plasma membrane though, paradoxically, works as an inhibitor of insulin exocytosis[48]. Nevertheless, we also observed a significant downregulation of the soluble N-ethyl maleimide sensitive factor associated receptor (SNARE) protein *Vamp3* (also known as cellubrevin) and an upregulation of *Syt1* (synaptotagmin 1), as well as *Syt17* and *Syt12*. Interplay between these, and potentially other, components of the docking/fusion machinery could contribute to the defective docking and secretion observed in these animals[49].

Additionally, many β-cell signature genes were down-regulated in MIR125B-Tg islets whereas neuronal genes were up-regulated. It is important to acknowledge that we cannot exclude the possibility that moderate fed hyperglycaemia in MIR125B-Tg mice indirectly contributes to the

loss of β-cell identity[36]. Ebrahimi and colleagues[50] have recently characterized in detail the changes in gene expression associated with mild and high hyperglycaemia. Most genes associated with β-cell identity that were downregulated in MIR125B-Tg islets, such as β-cell transcription factors (*Pdx1*, *Nkx6.1*, *Isl*), islet-associated polypeptide (*Iapp*) and GLUT2/*Slc2a2* were also downregulated by hyperglycaemia. Nevertheless, hyperglycaemia also up-regulated genes associated with epithelial-mesenchymal transition, inflammatory response, interleukin-6-Janus kinase (IL6-JaK-Stat3) signalling, apoptosis and several other pathways, none of whose genes were up-regulated in MIR125B-Tg islets. Also, key genes for β-cell function strongly downregulated by hyperglycaemia such as *Kcnj11* (ATP-dependent potassium channel), *Abcc8* (sulfonylurea receptor), *Gck* (glucokinase) and *Cacna1a* (voltage-dependent calcium channel subunits) were not significantly reduced in MIR125B-Tg, suggesting that the mild hyperglycaemia in these mice was not a major contributor to the effects observed in gene expression. It is also worth noting that the expression of the transgene, driven by rtTA under the control of a RIP7 promoter, is expected to occur as early as day (E) 11.5 and it is therefore possible that these defects are residual from impaired maturation rather than loss of identity. Interestingly, we have previously demonstrated that βAMPKdKO and βLKB1 islets present up-regulation of neuronal genes so it is tempting to hypothesize that increased miR-125b in these islets contribute to this phenotype.

It is worth mentioning that our findings contradict the work published in 2019 by Yu and colleagues[51]. Whereas both dishevelled binding antagonist of beta catenin 1 (*DACT1*) mRNA and β-cell proliferation remained unchanged upon miR-125 manipulation in all our experimental models, Yu and colleagues claimed miR-125b to have a positive effect on diabetic mouse β-cells through repressing DACT1 (at the mRNA level) and improving β-cell proliferation. A plausible explanation is the presence of other pancreatic, highly proliferative cells in the β-cell samples studied by these authors that observed unexpected doubling times of ~48h.

In the present study, we integrated RIP-seq and RNA-seq data[17, 21] of MIN6 cells transfected with control or miR-125 mimics which allowed us to identify dozens of miR-125b targets in an unbiased and high-throughput manner. One of the genes at the top of this list, *M6pr,* encodes the cation-dependent manose-6-phosphate protein MP6R (CD-M6PR). Even though the function of CD-M6PR has not been studied in β-cells, this receptor is necessary for adequate lysosomal targeting of several hydrolases, including β-hexosaminidase, β-galactosidase, β-glucuronidase and arylsulfatases [52 53], which were increasingly secreted in M6PR KO animals[52]. Remarkably, both miR-125b-overexpressing cells and MIR125B-Tg islets contained enlarged lysosomes/autophagolysosomes. Importantly, the presence of these structures can represent increased lysosomal function or, most probably, the accumulation of undigested cargos, including autophagic and endocytic substrates. Similar to our MIR125B-Tg islets, Masini et al. [54], observed enlarged autophagosomes in T2D islet micrographs. Whereas a decrease in macroautophagy has been suggested in both type 1[55] and type 2[56] diabetes, in mouse models of diabetes an early compensatory increase in macroautophagy is followed by compromised autophagy. Also, elimination of essential autophagy genes results in glucose intolerance and reduced insulin in response to HFD-induced diabetes possibly through preventing the formation of amyloid plaques that often appear in T2D [57]. Early studies indicated that chronic high glucose promotes β-cell autophagy while AMPK negatively regulates autophagy[57]. Whether elevated miR-125b during hyperglycamia/loss of AMPK activity contribute to this process and how, remains to be studied.

Undigested cargoes that cannot be recycled can compromise the whole membrane trafficking system[58]. Importantly, lysosomal, Golgi, endosomal and ER pathways consistently appear on the top of significantly associated pathways with genes dysregulated upon modulation of miR-125b activity in both cell lines and mouse and human islets. Moreover, our RIP-RNA-seq experiments identified additional miR-125b targets involved in these processes. For example, *PGAP3* encodes a glycophosphatidylinositol (GPI)-specific phospholipase A2 expressed in the Golgi critical for the association of GPI-anchored proteins and lipid rafts[59] and thus the

regulation of signalling pathways[60]. Also, *VPS29*, *VPS4B* and *RAB17* are involved in endosomal function which plays a pivotal and often overlooked role in several aspects of β-cell function, including receptor trafficking, signalling and/or degradation (i.e. GLP1R[61], Glut2[62]) and recycling of calcium channels[63]. Another example is the lysosomal palmitoyl protein thioesterase-2 (*PPT2)* whose whole-body disruption causes a lysosomal storage disorder and neurodegeneration, though a role in the pancreatic islets has not been investigated[64].

It is also likely that the defects on the lysosomal/trafficking machinery affect the maturation, packaging and location of the secretory granules within the cell[65 66] and might contribute to the reduced insulin content and to the crystallization defects observed in the MIR125B-Tg mice. MIR125B-Tg islets contain a 30% reduction in the zinc transporter *Znt8* mRNA (p 0.007, padj 0.11), which may also contribute to defective granule crystallization[67].

Even though we had identified several genes encoding mitochondrial proteins (i.e. *Mtfp1*, *Tor2a*, *Taz, Gnpat*) as miR-125b targets in MIN6 cells, no mitochondrial defects were detected in the transgenic islets that had similar morphology, DNA content and ATP-increases in response to glucose than control islets. Further supporting a lack of mitochondrial phenotype, GO analysis of genes altered in MIR125B-Tg islets failed to identify enrichment of mitochondria-associated pathways. Nevertheless, 35 significantly downregulated genes (including *Gnpat*) were annotated to mitochondria, opening the possibility of a compensatory effects.

On the other hand, deletion of miR-125b in EndoCβ-H1 cells resulted in a strong alteration of mitochondrial morphology and in the expression of mitochondrial proteins, including the miR-125b targets *Mtfp1* and *Gnpat*. Although this is the first study to identify *Gnpat* as a miR-125b target, *Mtfp1* is targeted by miR-125b in monocytes to promote elongation of the mitochondrial network and apoptosis[68]. GNPAT acts to stabilize DRP1[69] , which is required for mitochondrial fission and which deletion in β-cells results in elongated mitochondria, reduced mitochondria autophagy and, notably, impaired insulin secretion[70],[72]. In line with these earlier studies,

EndoCβ-H1-MIR125B2-KO cells contained shorter, more circular mitochondria which correlated with increased GSIS in these cells. It has, however, been contested whether mitochondrial fragmentation promotes apoptosis or correlates with hyperglycaemia or diabetes[28]. For example, prevention of mitochondrial fusion as a result of deletion of mitofusin genes results in secretory deficiencies and hyperglycaemia likely due to increased β-cell apoptosis [71]. Nevertheless, we did not observe any differences in cellular death or number in EndoCβ-H1-MIR125B2-KO (data not shown). Moreover, no differences in *Ddit3* (CHOP) mRNA levels were identified in our RNA-seq data, suggesting an absence of mitochondrial-induced ER stress in the KO cells. Future experiments are required to determine whether defective mitochondria generated by excessive fission in EndoCβ-H1-MIR125B-KO cells are efficiently cleared by thanks to a concomitant improvement in lysosomal function and mitophagy, and whether the positive effects of miR-125b elimination in β-cell function persist under conditions of cellular stress.

In summary, our results suggest that β-cell miR-125b has the potential to act as a glucose-regulated metabolic switch between the lysosomal system and mitochondria dynamics. Our *in vitro* and *in vivo* results strongly indicate that non-targeted administration of miR-125b mimics will lead to defective β-cell function and worsen diabetes. In contrast, islet-specific inhibition of miR-125b has the potential to improve glycaemic outcomes and limit the deleterious effect of hyperglycamia in β-cell function. Future studies focussed on cell-specific targeting of miR-125b will be essential to confirm the potential therapeutic benefit of targeting this miRNA for the treatment of diabetes.

METHODS

Cells and islets culture

MIN6 cells were cultured in 4.5 g/L glucose Dulbecco's modified Eagle's medium (DMEM) containing 15% FBS, 2mM L-glutamine, 20nM HEPES and 50 μM β-mercaptoethanol. EndoC-βH1 cells were cultured in 1g/L glucose DMEM supplemented with 2% Bovine Serum Albumin

Fraction V, Fatty Acids Free, 10mM nicotinamide, 5.5µg/ml transferrin6.7 ng/ml sodium selenite and 50µM 2-mercaptoethanol[73]. Mouse pancreatic islets were isolated with collagenase as described previously [74] and allowed for recovery from digestion overnight in culture medium (RPMI 1640, 10% FBS, L-glutamine and 11mM glucose) or directly used for experiments. Human islets were cultured in RPMI 1640, 10% FBS, L-glutamine and 5.5 mM glucose. The characteristics of the human donors are shown in Sup Table 9. Cells and islets were mantained at 37°C with 95% O_2/ 5% CO_2. AMPK activation was performed with 20 mM compound 13 (C13)[75] and 50 mM compound 991[76] as indicated in the figure legends.

Plasmids generation

To generate adenovirus expressing miR-125b, a 426-nucleotide sequence containing pre-miR-125b was amplified by PCR from C57BL6/J mice genomic DNA with the primers 5'-AGGGAGCCAGGATGTAGTCA-3' and 5'-CGGGTCACCTGATCCCATCTA-3' and sub-cloned into pAdTrackCMV (pAd-MIR125B). Adenovirus were then generated using the AdEasy system[77]. Adenovirus containing the empty vector were used as controls.

As above, the PCR-amplified pre-miR-125b-containing region was subcloned into pBI-LTet to generate pBI-LTet-MIR125B.

For reporter assays, full length *Taz*, *M6pr*, *Tor2a1*, *Mtfp1* and *Gnpat* 3'UTRs and *Tnksbp1* and *Gnpat* CDS were amplified by PCR from MIN6 cDNA and subcloned into pmirGLO (Promega), downstream the *Firefly* ORF. MiR-125b binding sites in *M6pr* and *Mtfp1* were identified with TargetScan[78] and three and two point mutations were introduced, respectively, in the sequences complementary to the miR-125b seed using site directed mutagenesis with the primers (mutated ntds in bold): *M6PR:* 5'-CTCTCCTGCTGGCT**ACT**GGAAGTGTCTGACCC-3' and 5'-GGGTCAGACACTTCC**AGT**AGCCAGCAGGAGAG-3'; *Mtfp1*: 5'-GTATTTGGGACACTC**TA**GGCAGAGTCTCTGG-3' and 5'-CCAGAGACTCTGCC**TA**GAGTGTCCCAAATAC-3'.

All the constructs were verified by sequencing.

Transfection of miRNA mimics, siRNAs and plasmidic DNA

Cells were transfected at 60-80% confluence with 5 nM/1nM (MIN6, EndoCβ-H1, respectively) control or miR-125b mimics (Qiagen) or 50 nM of a mixture of four ONTARGETplus siRNAs against mouse Smad2, Smad3 or non-targeting (Horizon Discovery) as previously described[9, 30]. For luciferase assays MIN6 cells were plated at ~70% confluency in 48-well plates, and, the following day, transfected with 0.4µl Lipofectamine 2000(ThermoFisher Scientific), 5ng plasmid and 5nM control or miR-125b mimics. After 24 h, cells were lysed and luciferase activity determined with the Dual-Glo luciferase assay system (Promega, UK), following the manufacturer's instructions.

CRISPR-Cas9-mediated deletion of miR-125b in EndoCβ-H1 cells

MIR125B-1 and *MIR125B-2* sequences were downloaded from miRBase[79]. Using the website tool available at http://crispr.mit.edu/, we designed two independent pair of gRNAs targeting the seed region of the mature miR-125b and/or the regions in the pri/pre-miR-125b essential for DROSHA and/or DICER processing (Supplemental figure/table 4) as in[80]. Two different gRNA pairs targeting each locus were subcloned under an H1 and U6 promoter within a lentiviral vector in which hSpCas9 expression is driven by a RIP (rat *Insulin* promoter) using the cloning strategy described in Beucher and Cebola in Nature Protocol exchange (https://protocolexchange.researchsquare.com/article/nprot-7395). EndoCβ-H1 cells were transfected with lentivirus expressing these gRNAs and the hSpCas9 and integrating cells were selected by subculture in the presence of 4µg/ml puromycin, encoded by the vector. Cells infected with lentiviral vectors containing the RIP-hSpCas9 cassette but without gRNAs were used as control. RT-qPCR for mature miR-125b was performed to assess the levels of the mature miR-125b in the resultant cell populations. All the experiments were performed with controls and KO cell populations generated from at least three independent infections.

Generation and maintenance of transgenic mice

The cassette expressing miR-125b under the control of a rtTA-inducible promoter, was excised from pBI-LTet-MIR125B and used for pronuclear microinjection of C57BL6/J oocytes at the Centre for Transgenic Models, Basel (http://www.ctm-basel.ch/). A founder was obtained containing one copy of the transgene as determined by qPCR (data not shown) and bred for two generations with C57BL6/J wild-type to ensure unique transgene insertion. The resulting animals were bred with mice expressing the reverse tetracyclin-regulated transactivator (rtTA) under the control of the RIP7 promoter (RIP7-rtTA$^{+/+}$), selective for β-cells. Mice bearing the transgene (MIR125B-Tg: RIP7-rtTA$^{+/-}$, MIR125B Tg$^{+/-}$) and controls (Control: RIP7-rtTA$^{+/-}$) were born at the expected mendelian ratios (50% each) and were used in subsequent experiments. Doxycycline (0.5 g/L) was continuously administered to these animals and to their parents from the time of mating in the drinking water.

βAMPKdKO (AMPKα1fl/fl, AMPKα2fl/fl, Ins1-Cre+/-), control (AMPKα1fl/fl, AMPKα2fl/fl, Ins1-Cre-/-), βLKB1KO (LKB1fl/fl, Ins1-Cre+/-) and control (LKB1fl/fl, Ins1-Cre-/-) were previously generated and maintained as in [9, 14].

All animals were granted free access to standard chow diet or, when indicated, ketogenic diet (Ssniff, Germany). All the *in vivo* procedures were approved by the UK Home Office Animal Scientific Procedures Act, 1986 (Licences PPL 70/7349 and PA03F7F0F to I.L.).

RNA extraction, reverse transcription (RT) and qPCR

Total RNA was extracted using Trizol (Thermofisher) following manufacturer's instructions. RT-qPCR was performed as previously described[9] with miRCURY LNA RT and SYBR Green PCR miRNA kits and miRCURY LNA probes for miRNAs (Qiagen) and High-capacity cDNA transcription kit and Fast SYBR Green (Qiagen) for mRNA and pri-miRNAs. For the latter, an anchored oligo dT primer was used in the RT reaction. MiR-7d-3p and miR-573-3p were used as endogenous controls due to their high stability in our system[9].

MiRISC immunoprecipitation.

MiRISC-immunoprecipitation was performed as previously described[17]. Briefly, MIN6 cells were seeded in 15 cm dishes and transfected with 5 nM of control or miR-125b mimic for 24 h. Following transfection cells were washed in cold PBS, scraped in PBS and collected by centrifugation. Pellets were then resuspended in 500ul of lysis buffer (20mM Tris-HCl pH7.5, 150mM KCl, 0.5% NP40, 2mM EDTA, 1 mM NaF, , 160 U ml−1 RNAsin and protease inhibitors) and pre-cleared with Dynabeads Protein G beads (Thermo Fisher Scientific) for 2 h at 4°C. Precleared extract was incubated with Dynabeads Protein G beads conjugated with 6µg of mouse-anti-AGO2 (clone E12-1C9, Abnova) or mouse IgG (NXA931, Merck) and 1mg/ml of heparin for at 4˚C for 16 hours with end-over-end rotation. After washing, the beads-immunoprecipitate were treated with TURBO™ DNase (2 U/µL) (Thermo Fisher Scientific) and proteinase K (20mg/ml) (Thermo Fisher Scientific) for 20 min at room temperature. RNA was extracted using phenol/ chloroform and ethanol/sodium acetate precipitation.

RNA sequencing library preparation, sequencing and analysis

Quantity and integrity of total RNA from MIN6, EndoCβ-H1 and mouse islets was determined with an Agilent Bioanalyzer and mRNA enrichmed was performed from 500-1000ng of RNA using a NEBNext Poly(A) mRNA Magnetic Isolation Kit (NEB). Library preparation from mRNA and from miRISC-isolated RNA was performed using a NEBNext Ultra II Directional RNA Library Prep Kit for Illumina (NEB) and Universal i5 and i7 primers following manufacturer's instructions. Library preparation from human islets total RNA (200ng) was performed using a NEBNext Low Input RNA Library Prep kit (NEB). Sequencing was performed on a HiSeq4000 using 75 bp paired end reads according to Illumina specifications. For total mRNA ~25-40 million reads/sample and for miRISC RNA~12 million reads/sample were obtained. FastQC (http://www.bioinformatics.babraham.ac.uk/projects/fastqc/) was used to assess the quality of the reads obtained and reads were then mapped to the mouse or human transcriptome (GRCm38 and GRCh37, respectively) using Salmon v1.3.0[81]. Differential expression analysis was performed with the R package DESeq2[82].

For miRNA target identification, Total mRNA (T-RNA) and immunoprecipitated RNA (RIP-RNA) samples were treated as separate datasets and the two resulting gene lists of differential analysis were used to calculate the ratio of immunoprecipitated RNA to total mRNA (IP-RNA/T-RNA) for each gene detected in both datasets. Genes were ranked by RIP-RNA/T-RNA ratio and subjected to motif discovery and enrichment analysis in their 3'UTRs and CDS with cWords[22]. Cytoscape[83] was used to visualize genes with RIP-RNA/T-RNA >1.5 (arbitrary cut-off). Gene set enrichment analysis (GSEA) was performed for genes with a baseMean (average of the normalized count values) > 10 ranked by fold change in gene expression in human islets infected with pAd-MIR125B or pAd-empty (Control) virus against the curated KEGG gene sets collection from MSigDB (Molecular Signature Database). DAVID[25] was used for Gene Ontology enrichment analysis of genes differentially dysregulated (padj<0.1) in MIR125B-Tg islets, EndoCβ-H1 MIR125B2-KO and in MIN6 cells overexpressing miR-125b.

Immunoblot and Immunohistochemistry

For Western blotting, whole EndoCβ-H1 cells and mouse islets lysates were prepared in RIPA buffer. 5-15µg of EndoCβ-H1 total protein extract or 10-20 islets extract was submitted to SDS-PAGE electrophoresis and transferred to 0.2µM PVDF membranes. Membranes were incubated o/n with anti-M6PR (sc-365196 Santa Cruz Biotechnology) or anti-Insulin (L6B10, Cell Signalling).

Slides for immunohistochemistry were prepared from isolated pancreata and visualized as previously detailed[84]. For β-cell mass and proliferation measurements, slides were blotted with the following primary antibodies: anti-insulin (IR00261-2, 1:4; Agilent Techologies) and anti-glucagon (g2654, 1:100; Sigma) and/or anti-Ki67 (ab15580, 1:100 Abcam) antibodies and mounted using DAPI-containing Prolong Diamond (Life Technologies). To quantify apoptosis, pancreatic sections were submitted to terminal deoxynucleotidyl transferase dUTP nick-end labeling (TUNEL) assay using a DeadEnd Fluorometric TUNEL system kit (Promega) according to the manufacturer's instructions. Slides were visualized with an Axiovert 200M

microscope (Zeiss). ImageJ software was used to quantify the area positively stained for insulin and glucagon and the number of Insulin-, Ki67-, TUNEL- and DAPI-positive cells of all visible islets. For β-cell mass we calculated the percentage of pancreatic surface that was positive, as measured in whole pancreas sections separated by at least 25 µm in the z-axis. For β-to-α cell mass we calculated the ratio of insulin to glucagon positive area in all visible islets.

Electron microscopy

MIN6 and EndoCβ-H1 cells grown on Thermanox (Thermofisher Scientific) and whole isolated islets were fixed for 30 minutes or 2hrs, respectively, at room temperature in suspension with 2% paraformaldehyde (EM grade), 2% glutaraldehyde, and 3 mM CaCl2 in 0.1 M cacodylate buffer before post-fixation and embedding for conventional electron microscopy as in Jones et al[85]. Ultrathin 70-nm sections were cut using a Leica ultramicrotome prior to examination in a Tecnai Spirit or JEOL 1400 plus transmission electron microscopes. Images at 2000x magnification were subsequently analysed in ImageJ as in Pasquier et al. [86], with quantifications performed blindly.

Intraperitoneal Glucose and Insulin tolerance tests (IPGG, ITT) and *In vivo* Insulin secretion

Mice were fasted overnight (IPGTT) or for 5h (ITT) prior the administration of 1g/kg body weight (IPGTT) or 1.2U/kg exogenous insulin (NovoRapid, ITT). Blood glucose measurement was recorded at time point 0 (basal glucose) and 15, 30, 60 and 120 minutes post-injection from the tail vein, using an automatic glucometer (Contour). For insulin secretion, mice were fasted overnight and injected with 3g/kg body weight glucose. EDTA coated tubes (Sarsdtedt) were used to collect blood from the tail vein from mice at time 0 (basal glucose) and 15 minutes post-injection. Plasma was separated by centrifugation at 2000 x g for 20 minutes. Insulin levels were measured using an ultra-sensitive mouse insulin enzyme-linked immunosorbent assay (ELISA kit; Crystal Chem, Netherlands).

Insulin secretion (*In vitro*):

15 size-matched islets per condition, in triplicates, were pre-incubated for 1 hour at 37°C in a Krebs-Ringer-bicarbonate Hepes (KRBH) solution (140mM NaCl, 3.6mM KCL, 1.5mM CaCl2, 0.5mM MgSO4, 0.5mM Na2PO4, 2mM NaHCO3, 10mM HEPES and 0.1% [wt/vol] BSA, bubbled with 95% O2/5% CO2 for ~20 minutes and adjusted to pH 7.4) containing 3mM glucose. Islets were subsequently transferred to Eppendorf tubes and sequentially incubated with 3mM, 17 mM glucose or 3mM glucose plus 20 mM KCl for 30 minutes. Supernatant containing secreted insulin was collected for analysis and whole islets were lysed in 500ul acidified ethanol solution. Secreted insulin and total insulin were quantified using an HTRF insulin kit (Cisbio) in a PHERAstar reader (BMG Labtech, UK) following the manufacturer's guidelines.

Insulin secretion from MIN6 and EndoCβ-H1 cells was performed as above with the following modifications: cells were seeded at 70% confluence 48h ahead of the assay and kept at 3mM glucose overnight before the experiment. Cells were incubated in KRBH containing 3mM or 0.5mM Glucose for 1h and stimulated with 17 or 15 mM glucose (MIN6 and EndoCβ-H1, respectively) for 1h as previously described [30, 73].

Islet fluorescence imaging

For Ca^{2+} Imaging, whole isolated islets were incubated with Cal-520 (4.5uM; Stratech) for 45 min at 37 °C in KRBH containing 3mM glucose. For ATP imaging, 48 hours prior to experiment, islets were infected with an adenovirus containing encoding the ATP sensor Perceval[87]. Islets were incubated in KRBH buffer supplemented with 3mM glucose for 45 minutes before imaging. Excitation of the probes was achieved using 491nm and emitted light was filtered at 525nm. Islets were kept at 37°C and constantly perifused with KRBH B containing 3mM or 17mM glucose or 20mM KCl. Fluorescence live imaging was performed using a Nipkow spinning disk head and Velocity software (PerkinElmer). Data were analyzed with ImageJ software using an in-house-made macro, available upon request.

For TIRF experiments, mouse islet were infected with an adenovirus construct for NPY-venus 48 hour prior to the experiments. Before imaging, islets were dissociated using accutase, pelleted, resuspended in normal culture media and left to attach on a glass slide treated with polylysine. After incubation in KRBH buffer containing 3 mM glucose, slide was mounted in an imaging chamber. Imaging of cells expressing NPY-venus in the secreting vesicle was performed as described previously[88] using a Nikon Eclipse Ti microscope equipped with a ×100/1.49 numerical aperture (NA) TIRF objective, a TIRF iLas2 module to control laser angle (Roper Scientific), and a Quad Band TIRF filter cube (TRF89902, Chroma). Acquisitions were performed using a 488-nm laser line, and images were captured with an ORCA-Flash 4.0 camera (Hamamatsu). Metamorph software (Molecular Devices) was used for data capture, acquisition speed was set at 3Hz and the laser angle was selected for an imaged section thickness at the cell membrane of 150–180 nm. KCl at 20mM was used to stimulate insulin secretion and added to the well during acquisition after 3 minutes in KRBH 3 mM Glucose. Image analysis was performed using ImageJ to measure mean fluorescence intensity at the cell membrane over time.

For mitochondria morphology analysis MIN6 and EndoCβ-H1 cells and dissociated mouse islets cultured in coverslips were pre-incubated for 45 minutes in KRBH solution supplemented with 25, 5 or 11 mM glucose, respectively, and Mitotracker Green™ (100nM for MIN6 and islets, 70nM for EndoCβ-H1; ThermoFisher) in a 37ºC humidified incubator with 95% O_2/5% CO_2. Mitotracker green was washed with KRBH buffer before imaging. Cell images were acquired with a 60x oil immersion objective lens (Olympus) in a Nikon ECLIPSE Ti microscope. Dissociated islets were imaged on a LSM780 inverted confocal microscope (Carl Zeiss, Cambridge, UK) using a ×63 1.4 numerical aperture (NA) oil objective. Two to three randomly selected fields of view were taken per acquisition, containing 5-15 MIN6/EndoCβ-H1 cells or a single dissociated mouse β-cell. Images were deconvoluted using Huygens software (Scientific Volume Imaging). Mitochondria morphological characteristics (i.e. number, area, elongation, circularity and perimeter) were quantified with ImageJ using an in-house

macro (available upon request) as described by Wiemerslage et al [89]. Quantifications were performed in z-stacks of 10 images for EndoC-βH1 and MIN6 cells and in three stacks of three images each at the top, middle and bottom of the primary β-cells.

Mitochondria DNA / Nuclear DNA (mtDNA/nDNA) ratio analysis

DNA from islets was extracted with SNET buffer (20mM TRIS pH 8.0, 5mM EDTA pH 8.0, 400mM NaCl, 1% SDS) supplemented with 40ug/ml Proteinase K. qPCR was performed with Fast SYBR-Green (Life Technologies) and primers for mitochondrial DNA (Mt9/Mt11 5'-GAGCATCTTATCCACGCTTCC-3' and 5'-GGTGGTACTCCCGCTGTAAA-3') and genomic DNA (Cxcl12, 5'-CGGTAGGAGGTTTACAGCATGA-3' and 5'-GGTGTCAGCCACGGTGTATT-3').

Statistical analysis

Statistical significance was evaluated with GraphPad Prism 9.0 software as indicated in the Figure legends. All data are shown as means ± SEM. $p < 0.05$ was considered statistically significant unless otherwise specified.

AUTHOR CONTRIBUTIONS

R. Cheung & G.Pizza (equal contribution) performed most experiments, designed research studies and obtained and analyzed data; P. Chabosseau performed research studies (TIRF) and designed microscopy macros. D. Rolando assisted with computational analysis of RNA-seq and RIP-seq data. A. Tomas and T. Burgoyne performed TEM experiments. A. Salowka, A. Macklin and Y. Cao performed research studies (β-cell mass and apoptosis and Western blot, respectively). M.-S. Nguyen-Tu assisted with animal studies (*In vivo* Insulin secretion). P. Marchetti, J.Shapiro, L. Piemonti and E. de Koning, provided human islets. I. Leclerc assisted with maintenance of animal colonies. K. Sakamoto and D. M. Smith provided C13 and C991, respectively. G. A. Rutter contributed to the study design, with reagents and AMPK and LKB1 KO animals, and in writing the manuscript. A. Martinez-Sanchez conceived the study, designed and performed experiments, analyzed data, and wrote the paper; All authors

read and approved the manuscript. A. Martinez-Sanchez is the guarantor of this work and, as such, had full access to all the data in the study and takes responsibility for the integrity of the data and the accuracy of the data analysis.

ACKNOLEDMENTS & FUNDING

The authors thank Stephen M. Rothery from the Facility for Imaging by Light Microscopy (FILM) at Imperial College London for support with confocal and widefield microscopy image acquisition and analysis. A.M-S was supported by an MRC New Investigator Research Grant MR/P023223/1. G.A.R. was supported by a Wellcome Trust Senior Investigator Award (WT098424AIA) and Investigator Award (212625/Z/18/Z) and MRC Programme grants (MR/R022259/1,MR/J0003042/1, MR/L020149/1). A.T was funded by the MRC (MR/R010676/1). IL was supported by a Diabetes UK project grant (16/0005485). This project has received funding from the European Union's Horizon 2020 research and innovation programme via the Innovative Medicines Initiative 2 Joint Undertaking under grant agreement No. 115881 (RHAPSODY) to G.R. and P.M. Human islet preparations (Milan, Italy) were obtained from the European Consortium for Islet Transplantation; the Human Islet Distribution program was supported by Juvenile Diabetes Research Foundation Grant 3-RSC-2016-160-I-X.. The authors declare no conflicts of interest

1. Rutter, G. A.; Pullen, T. J.; Hodson, D. J.; Martinez-Sanchez, A., Pancreatic beta cell identity, glucose sensing and the control of insulin secretion. Biochem J, 2015; Vol. 466, pp 202-218.
2. Talchai, C.; Xuan, S.; Lin, H. V.; Sussel, L.; Accili, D., Pancreatic beta cell dedifferentiation as a mechanism of diabetic beta cell failure. *Cell* **2012,** *150* (6), 1223-34.
3. Rahier, J.; Guiot, Y.; Goebbels, R. M.; Sempoux, C.; Henquin, J. C., Pancreatic beta-cell mass in European subjects with type 2 diabetes. *Diabetes Obes Metab* **2008,** *10 Suppl 4*, 32-42.
4. Chen, C.; Cohrs, C. M.; Stertmann, J.; Bozsak, R.; Speier, S., Human beta cell mass and function in diabetes: Recent advances in knowledge and technologies to understand disease pathogenesis. *Mol Metab* **2017,** *6* (9), 943-957.
5. Swisa, A.; Glaser, B.; Dor, Y., Metabolic Stress and Compromised Identity of Pancreatic Beta Cells. *Front Genet* **2017,** *8*, 21.
6. Sun, K.; Lai, E. C., Adult-specific functions of animal microRNAs. *Nat Rev Genet* **2013,** *14* (8), 535-48.
7. Martinez-Sanchez, A.; Rutter, G. A.; Latreille, M., MiRNAs in β-Cell Development, Identity, and Disease. *Front Genet* **2016,** *7*, 226.

8. Sun, Y. M.; Lin, K. Y.; Chen, Y. Q., Diverse functions of miR-125 family in different cell contexts. *J Hematol Oncol* **2013,** *6*, 6.
9. Martinez-Sanchez, A.; Nguyen-Tu, M. S.; Cebola, I.; Yavari, A.; Marchetti, P.; Piemonti, L.; de Koning, E.; Shapiro, A. M. J.; Johnson, P.; Sakamoto, K.; Smith, D. M.; Leclerc, I.; Ashrafian, H.; Ferrer, J.; Rutter, G. A., MiR-184 expression is regulated by AMPK in pancreatic islets. *FASEB J* **2018,** *32* (5), 2587-2600.
10. Salt, I. P.; Johnson, G.; Ashcroft, S. J.; Hardie, D. G., AMP-activated protein kinase is activated by low glucose in cell lines derived from pancreatic beta cells, and may regulate insulin release. *Biochem J* **1998,** *335 (Pt 3)*, 533-9.
11. Del Guerra, S.; Lupi, R.; Marselli, L.; Masini, M.; Bugliani, M.; Sbrana, S.; Torri, S.; Pollera, M.; Boggi, U.; Mosca, F.; Del Prato, S.; Marchetti, P., Functional and molecular defects of pancreatic islets in human type 2 diabetes. *Diabetes* **2005,** *54* (3), 727-35.
12. Jaafar, R.; Tran, S.; Shah, A. N.; Sun, G.; Valdearcos, M.; Marchetti, P.; Masini, M.; Swisa, A.; Giacometti, S.; Bernal-Mizrachi, E.; Matveyenko, A.; Hebrok, M.; Dor, Y.; Rutter, G. A.; Koliwad, S. K.; Bhushan, A., mTORC1 to AMPK switching underlies β-cell metabolic plasticity during maturation and diabetes. *J Clin Invest* **2019,** *129* (10), 4124-4137.
13. Yi, S. W.; Park, S.; Lee, Y. H.; Park, H. J.; Balkau, B.; Yi, J. J., Association between fasting glucose and all-cause mortality according to sex and age: a prospective cohort study. *Sci Rep* **2017,** *7* (1), 8194.
14. Kone, M.; Pullen, T. J.; Sun, G.; Ibberson, M.; Martinez-Sanchez, A.; Sayers, S.; Nguyen-Tu, M. S.; Kantor, C.; Swisa, A.; Dor, Y.; Gorman, T.; Ferrer, J.; Thorens, B.; Reimann, F.; Gribble, F.; McGinty, J. A.; Chen, L.; French, P. M.; Birzele, F.; Hildebrandt, T.; Uphues, I.; Rutter, G. A., LKB1 and AMPK differentially regulate pancreatic beta-cell identity. *Faseb j* **2014,** *28* (11), 4972-85.
15. Gulyaeva, L. F.; Kushlinskiy, N. E., Regulatory mechanisms of microRNA expression. *J Transl Med* **2016,** *14* (1), 143.
16. de Rie, D.; Abugessaisa, I.; Alam, T.; Arner, E.; Arner, P.; Ashoor, H.; Åström, G.; Babina, M.; Bertin, N.; Burroughs, A. M.; Carlisle, A. J.; Daub, C. O.; Detmar, M.; Deviatiiarov, R.; Fort, A.; Gebhard, C.; Goldowitz, D.; Guhl, S.; Ha, T. J.; Harshbarger, J.; Hasegawa, A.; Hashimoto, K.; Herlyn, M.; Heutink, P.; Hitchens, K. J.; Hon, C. C.; Huang, E.; Ishizu, Y.; Kai, C.; Kasukawa, T.; Klinken, P.; Lassmann, T.; Lecellier, C. H.; Lee, W.; Lizio, M.; Makeev, V.; Mathelier, A.; Medvedeva, Y. A.; Mejhert, N.; Mungall, C. J.; Noma, S.; Ohshima, M.; Okada-Hatakeyama, M.; Persson, H.; Rizzu, P.; Roudnicky, F.; Sætrom, P.; Sato, H.; Severin, J.; Shin, J. W.; Swoboda, R. K.; Tarui, H.; Toyoda, H.; Vitting-Seerup, K.; Winteringham, L.; Yamaguchi, Y.; Yasuzawa, K.; Yoneda, M.; Yumoto, N.; Zabierowski, S.; Zhang, P. G.; Wells, C. A.; Summers, K. M.; Kawaji, H.; Sandelin, A.; Rehli, M.; Hayashizaki, Y.; Carninci, P.; Forrest, A. R. R.; de Hoon, M. J. L.; Consortium, F., An integrated expression atlas of miRNAs and their promoters in human and mouse. *Nat Biotechnol* **2017,** *35* (9), 872-878.
17. Ottaviani, S.; Stebbing, J.; Frampton, A. E.; Zagorac, S.; Krell, J.; de Giorgio, A.; Trabulo, S. M.; Nguyen, V. T. M.; Magnani, L.; Feng, H.; Giovannetti, E.; Funel, N.; Gress, T. M.; Jiao, L. R.; Lombardo, Y.; Lemoine, N. R.; Heeschen, C.; Castellano, L., TGF-β induces miR-100 and miR-125b but blocks let-7a through LIN28B controlling PDAC progression. *Nat Commun* **2018,** *9* (1), 1845.
18. Scharfmann, R.; Pechberty, S.; Hazhouz, Y.; von Bülow, M.; Bricout-Neveu, E.; Grenier-Godard, M.; Guez, F.; Rachdi, L.; Lohmann, M.; Czernichow, P.; Ravassard, P., Development of a conditionally immortalized human pancreatic β cell line. *J Clin Invest* **2014,** *124* (5), 2087-98.
19. Bartel, D. P., MicroRNAs: target recognition and regulatory functions. *Cell* **2009,** *136* (2), 215-33.
20. Eichhorn, S. W.; Guo, H.; McGeary, S. E.; Rodriguez-Mias, R. A.; Shin, C.; Baek, D.; Hsu, S. H.; Ghoshal, K.; Villén, J.; Bartel, D. P., mRNA destabilization is the dominant effect of mammalian microRNAs by the time substantial repression ensues. *Mol Cell* **2014,** *56* (1), 104-15.

21. Martinez-Sanchez, A.; Lazzarano, S.; Sharma, E.; Lockstone, H.; Murphy, C. L., High-Throughput Identification of MiR-145 Targets in Human Articular Chondrocytes. *Life (Basel)* **2020,** *10* (5).
22. Rasmussen, S. H.; Jacobsen, A.; Krogh, A., cWords - systematic microRNA regulatory motif discovery from mRNA expression data. *Silence* **2013,** *4* (1), 2.
23. Martinez-Sanchez, A.; Murphy, C. L., MicroRNA Target Identification-Experimental Approaches. *Biology (Basel)* **2013,** *2* (1), 189-205.
24. Zhang, K.; Zhang, X.; Cai, Z.; Zhou, J.; Cao, R.; Zhao, Y.; Chen, Z.; Wang, D.; Ruan, W.; Zhao, Q.; Liu, G.; Xue, Y.; Qin, Y.; Zhou, B.; Wu, L.; Nilsen, T.; Zhou, Y.; Fu, X. D., A novel class of microRNA-recognition elements that function only within open reading frames. *Nat Struct Mol Biol* **2018,** *25* (11), 1019-1027.
25. Huang, d. W.; Sherman, B. T.; Lempicki, R. A., Systematic and integrative analysis of large gene lists using DAVID bioinformatics resources. *Nat Protoc* **2009,** *4* (1), 44-57.
26. Schweizer, A.; Kornfeld, S.; Rohrer, J., Proper sorting of the cation-dependent mannose 6-phosphate receptor in endosomes depends on a pair of aromatic amino acids in its cytoplasmic tail. *Proc Natl Acad Sci U S A* **1997,** *94* (26), 14471-6.
27. Tondera, D.; Czauderna, F.; Paulick, K.; Schwarzer, R.; Kaufmann, J.; Santel, A., The mitochondrial protein MTP18 contributes to mitochondrial fission in mammalian cells. *J Cell Sci* **2005,** *118* (Pt 14), 3049-59.
28. Wada, J.; Nakatsuka, A., Mitochondrial Dynamics and Mitochondrial Dysfunction in Diabetes. *Acta Med Okayama* **2016,** *70* (3), 151-8.
29. Licursi, V.; Conte, F.; Fiscon, G.; Paci, P., MIENTURNET: an interactive web tool for microRNA-target enrichment and network-based analysis. *BMC Bioinformatics* **2019,** *20* (1), 545.
30. Martinez-Sanchez, A.; Pullen, T. J.; Chabosseau, P.; Zhang, Q.; Haythorne, E.; Cane, M. C.; Nguyen-Tu, M. S.; Sayers, S. R.; Rutter, G. A., Disallowance of Acot7 in beta-Cells Is Required for Normal Glucose Tolerance and Insulin Secretion. *Diabetes* **2016,** *65* (5), 1268-82.
31. Wicksteed, B.; Brissova, M.; Yan, W.; Opland, D. M.; Plank, J. L.; Reinert, R. B.; Dickson, L. M.; Tamarina, N. A.; Philipson, L. H.; Shostak, A.; Bernal-Mizrachi, E.; Elghazi, L.; Roe, M. W.; Labosky, P. A.; Myers, M. G.; Gannon, M.; Powers, A. C.; Dempsey, P. J., Conditional gene targeting in mouse pancreatic ß-Cells: analysis of ectopic Cre transgene expression in the brain. *Diabetes* **2010,** *59* (12), 3090-8.
32. Tsuboi, T.; Ravier, M. A.; Parton, L. E.; Rutter, G. A., Sustained Exposure to High Glucose Concentrations Modifies Glucose Signaling and the Mechanics of Secretory Vesicle Fusion in Primary Rat Pancreatic -Cells. *Diabetes* **2006,** *55* (4), 1057-1065.
33. Busby, M. A.; Stewart, C.; Miller, C. A.; Grzeda, K. R.; Marth, G. T., Scotty: a web tool for designing RNA-Seq experiments to measure differential gene expression. *Bioinformatics* **2013,** *29* (5), 656-7.
34. Klein, D.; Misawa, R.; Bravo-Egana, V.; Vargas, N.; Rosero, S.; Piroso, J.; Ichii, H.; Umland, O.; Zhijie, J.; Tsinoremas, N.; Ricordi, C.; Inverardi, L.; Domínguez-Bendala, J.; Pastori, R. L., MicroRNA expression in alpha and beta cells of human pancreatic islets. *PLoS One* **2013,** *8* (1), e55064.
35. White, M. G.; Shaw, J. A.; Taylor, R., Type 2 Diabetes: The Pathologic Basis of Reversible β-Cell Dysfunction. *Diabetes Care* **2016,** *39* (11), 2080-2088.
36. Brereton, M. F.; Rohm, M.; Shimomura, K.; Holland, C.; Tornovsky-Babeay, S.; Dadon, D.; Iberl, M.; Chibalina, M. V.; Lee, S.; Glaser, B.; Dor, Y.; Rorsman, P.; Clark, A.; Ashcroft, F. M., Hyperglycaemia induces metabolic dysfunction and glycogen accumulation in pancreatic β-cells. *Nat Commun* **2016,** *7*, 13496.
37. Satake, E.; Pezzolesi, M. G.; Md Dom, Z. I.; Smiles, A. M.; Niewczas, M. A.; Krolewski, A. S., Circulating miRNA Profiles Associated With Hyperglycemia in Patients With Type 1 Diabetes. *Diabetes* **2018,** *67* (5), 1013-1023.

38. de Candia, P.; Spinetti, G.; Specchia, C.; Sangalli, E.; La Sala, L.; Uccellatore, A.; Lupini, S.; Genovese, S.; Matarese, G.; Ceriello, A., A unique plasma microRNA profile defines type 2 diabetes progression. *PLoS One* **2017,** *12* (12), e0188980.
39. Lamadrid-Romero, M.; Solís, K. H.; Cruz-Reséndiz, M. S.; Pérez, J. E.; Díaz, N. F.; Flores-Herrera, H.; García-López, G.; Perichart, O.; Reyes-Muñoz, E.; Arenas-Huertero, F.; Eguía-Aguilar, P.; Molina-Hernández, A., Central nervous system development-related microRNAs levels increase in the serum of gestational diabetic women during the first trimester of pregnancy. *Neurosci Res* **2018,** *130*, 8-22.
40. Wei, L. M.; Sun, R. P.; Dong, T.; Liu, J.; Chen, T.; Zeng, B.; Wu, J. H.; Luo, J. Y.; Sun, J. J.; Xi, Q. Y.; Zhang, Y. L., MiR-125b-2 knockout increases high-fat diet-induced fat accumulation and insulin resistance. *Sci Rep* **2020,** *10* (1), 21969.
41. Strycharz, J.; Wróblewski, A.; Zieleniak, A.; Świderska, E.; Matyjas, T.; Rucińska, M.; Pomorski, L.; Czarny, P.; Szemraj, J.; Drzewoski, J.; Śliwińska, A., Visceral Adipose Tissue of Prediabetic and Diabetic Females Shares a Set of Similarly Upregulated microRNAs Functionally Annotated to Inflammation, Oxidative Stress and Insulin Signaling. *Antioxidants (Basel)* **2021,** *10* (1).
42. Giroud, M.; Pisani, D. F.; Karbiener, M.; Barquissau, V.; Ghandour, R. A.; Tews, D.; Fischer-Posovszky, P.; Chambard, J. C.; Knippschild, U.; Niemi, T.; Taittonen, M.; Nuutila, P.; Wabitsch, M.; Herzig, S.; Virtanen, K. A.; Langin, D.; Scheideler, M.; Amri, E. Z., miR-125b affects mitochondrial biogenesis and impairs brite adipocyte formation and function. *Mol Metab* **2016,** *5* (8), 615-625.
43. Du, X.; Li, X.; Chen, L.; Zhang, M.; Lei, L.; Gao, W.; Shi, Z.; Dong, Y.; Wang, Z.; Liu, G., Hepatic miR-125b inhibits insulin signaling pathway by targeting PIK3CD. *J Cell Physiol* **2018,** *233* (8), 6052-6066.
44. Kalwat, M. A.; Cobb, M. H., Mechanisms of the amplifying pathway of insulin secretion in the β cell. *Pharmacol Ther* **2017,** *179*, 17-30.
45. Gooding, J. R.; Jensen, M. V.; Dai, X.; Wenner, B. R.; Lu, D.; Arumugam, R.; Ferdaoussi, M.; MacDonald, P. E.; Newgard, C. B., Adenylosuccinate Is an Insulin Secretagogue Derived from Glucose-Induced Purine Metabolism. *Cell Rep* **2015,** *13* (1), 157-167.
46. Li, C.; Buettger, C.; Kwagh, J.; Matter, A.; Daikhin, Y.; Nissim, I. B.; Collins, H. W.; Yudkoff, M.; Stanley, C. A.; Matschinsky, F. M., A signaling role of glutamine in insulin secretion. *J Biol Chem* **2004,** *279* (14), 13393-401.
47. Han, G.; Takahashi, H.; Murao, N.; Gheni, G.; Yokoi, N.; Hamamoto, Y.; Asahara, S. I.; Seino, Y.; Kido, Y.; Seino, S., Glutamate is an essential mediator in glutamine-amplified insulin secretion. *J Diabetes Investig* **2021**.
48. Kato, T.; Shimano, H.; Yamamoto, T.; Yokoo, T.; Endo, Y.; Ishikawa, M.; Matsuzaka, T.; Nakagawa, Y.; Kumadaki, S.; Yahagi, N.; Takahashi, A.; Sone, H.; Suzuki, H.; Toyoshima, H.; Hasty, A. H.; Takahashi, S.; Gomi, H.; Izumi, T.; Yamada, N., Granuphilin is activated by SREBP-1c and involved in impaired insulin secretion in diabetic mice. *Cell Metab* **2006,** *4* (2), 143-54.
49. Kreutzberger, A. J. B.; Kiessling, V.; Doyle, C. A.; Schenk, N.; Upchurch, C. M.; Elmer-Dixon, M.; Ward, A. E.; Preobraschenski, J.; Hussein, S. S.; Tomaka, W.; Seelheim, P.; Kattan, I.; Harris, M.; Liang, B.; Kenworthy, A. K.; Desai, B. N.; Leitinger, N.; Anantharam, A.; Castle, J. D.; Tamm, L. K., Distinct insulin granule subpopulations implicated in the secretory pathology of diabetes types 1 and 2. *Elife* **2020,** *9*.
50. Ebrahimi, A. G.; Hollister-Lock, J.; Sullivan, B. A.; Tsuchida, R.; Bonner-Weir, S.; Weir, G. C., Beta cell identity changes with mild hyperglycemia: Implications for function, growth, and vulnerability. *Mol Metab* **2020,** *35*, 100959.
51. Yu, C. Y.; Yang, C. Y.; Rui, Z. L., MicroRNA-125b-5p improves pancreatic β-cell function through inhibiting JNK signaling pathway by targeting DACT1 in mice with type 2 diabetes mellitus. *Life Sci* **2019,** *224*, 67-75.
52. Ludwig, T.; Ovitt, C. E.; Bauer, U.; Hollinshead, M.; Remmler, J.; Lobel, P.; Rüther, U.; Hoflack, B., Targeted disruption of the mouse cation-dependent mannose 6-phosphate receptor results in partial missorting of multiple lysosomal enzymes. *EMBO J* **1993,** *12* (13), 5225-35.

53. Baldwin, A. C.; Naatz, A.; Bohnsack, R. N.; Bartosiak, J. T.; Oleson, B. J.; Hansen, P. A.; Dahms, N. M.; Corbett, J. A., Cation-Independent Mannose 6-Phosphate Receptor Deficiency Enhances β-Cell Susceptibility to Palmitate. *Mol Cell Biol* **2018,** *38* (8).
54. Masini, M.; Bugliani, M.; Lupi, R.; del Guerra, S.; Boggi, U.; Filipponi, F.; Marselli, L.; Masiello, P.; Marchetti, P., Autophagy in human type 2 diabetes pancreatic beta cells. *Diabetologia* **2009,** *52* (6), 1083-6.
55. Muralidharan, C.; Conteh, A. M.; Marasco, M. R.; Crowder, J. J.; Kuipers, J.; de Boer, P.; Linnemann, A. K., Pancreatic beta cell autophagy is impaired in type 1 diabetes. *Diabetologia* **2021,** *64* (4), 865-877.
56. Mizukami, H.; Takahashi, K.; Inaba, W.; Tsuboi, K.; Osonoi, S.; Yoshida, T.; Yagihashi, S., Involvement of oxidative stress-induced DNA damage, endoplasmic reticulum stress, and autophagy deficits in the decline of β-cell mass in Japanese type 2 diabetic patients. *Diabetes Care* **2014,** *37* (7), 1966-74.
57. Mészáros, G.; Pasquier, A.; Vivot, K.; Goginashvili, A.; Ricci, R., Lysosomes in nutrient signalling: A focus on pancreatic β-cells. *Diabetes Obes Metab* **2018,** *20 Suppl 2*, 104-115.
58. Xu, H.; Ren, D., Lysosomal physiology. *Annu Rev Physiol* **2015,** *77*, 57-80.
59. Muñiz, M.; Riezman, H., Trafficking of glycosylphosphatidylinositol anchored proteins from the endoplasmic reticulum to the cell surface. *J Lipid Res* **2016,** *57* (3), 352-60.
60. Manea, E., A step closer in defining glycosylphosphatidylinositol anchored proteins role in health and glycosylation disorders. *Mol Genet Metab Rep* **2018,** *16*, 67-75.
61. Fang, Z.; Chen, S.; Manchanda, Y.; Bitsi, S.; Pickford, P.; David, A.; Shchepinova, M. M.; Corrêa, I. R.; Hodson, D. J.; Broichhagen, J.; Tate, E. W.; Reimann, F.; Salem, V.; Rutter, G. A.; Tan, T.; Bloom, S. R.; Tomas, A.; Jones, B., Ligand-Specific Factors Influencing GLP-1 Receptor Post-Endocytic Trafficking and Degradation in Pancreatic Beta Cells. *Int J Mol Sci* **2020,** *21* (21).
62. Ding, L.; Han, L.; Dube, J.; Billadeau, D. D., WASH Regulates Glucose Homeostasis by Facilitating Glut2 Receptor Recycling in Pancreatic β-Cells. *Diabetes* **2019,** *68* (2), 377-386.
63. Ye, Y.; Barghouth, M.; Luan, C.; Kazim, A.; Zhou, Y.; Eliasson, L.; Zhang, E.; Hansson, O.; Thevenin, T.; Renström, E., The TCF7L2-dependent high-voltage activated calcium channel subunit α2δ-1 controls calcium signaling in rodent pancreatic beta-cells. *Mol Cell Endocrinol* **2020,** *502*, 110673.
64. Gupta, P.; Soyombo, A. A.; Shelton, J. M.; Wilkofsky, I. G.; Wisniewski, K. E.; Richardson, J. A.; Hofmann, S. L., Disruption of PPT2 in mice causes an unusual lysosomal storage disorder with neurovisceral features. *Proc Natl Acad Sci U S A* **2003,** *100* (21), 12325-30.
65. Omar-Hmeadi, M.; Idevall-Hagren, O., Insulin granule biogenesis and exocytosis. *Cell Mol Life Sci* **2020**.
66. Arvan, P.; Halban, P. A., Sorting ourselves out: seeking consensus on trafficking in the beta-cell. *Traffic* **2004,** *5* (1), 53-61.
67. Mitchell, R. K.; Hu, M.; Chabosseau, P. L.; Cane, M. C.; Meur, G.; Bellomo, E. A.; Carzaniga, R.; Collinson, L. M.; Li, W.-H.; Hodson, D. J.; Rutter, G. A., Molecular Genetic Regulation ofSlc30a8/ZnT8 Reveals a Positive Association With Glucose Tolerance.
68. Duroux-Richard, I.; Roubert, C.; Ammari, M.; Présumey, J.; Grün, J. R.; Häupl, T.; Grützkau, A.; Lecellier, C. H.; Boitez, V.; Codogno, P.; Escoubet, J.; Pers, Y. M.; Jorgensen, C.; Apparailly, F., miR-125b controls monocyte adaptation to inflammation through mitochondrial metabolism and dynamics. *Blood* **2016,** *128* (26), 3125-3136.
69. Gu, L.; Zhu, Y.; Lin, X.; Li, Y.; Cui, K.; Prochownik, E. V., Amplification of Glyceronephosphate O-Acyltransferase and Recruitment of USP30 Stabilize DRP1 to Promote Hepatocarcinogenesis. *Cancer Res* **2018,** *78* (20), 5808-5819.
70. Hennings, T. G.; Chopra, D. G.; DeLeon, E. R.; VanDeusen, H. R.; Sesaki, H.; Merrins, M. J.; Ku, G. M., In Vivo Deletion of β-Cell Drp1 Impairs Insulin Secretion Without Affecting Islet Oxygen Consumption. *Endocrinology* **2018,** *159* (9), 3245-3256.

71. Georgiadou, E.; Muralidharan, C.; Martinez, M.; Chabosseau, P.; Tomas, A.; Su Wern, F. Y.; Stylianides, T.; Rothery, S. M.; Di Gregorio, A.; Leclerc, I.; Ali, Y.; Linnemann, A. K.; Rodriguez, T. A.; Rutter, G. A., Pancreatic beta cell selective deletion of mitofusins 1 and 2 (Mfn1 and Mfn2) disrupts mitochondrial architecture and abrogates glucose-stimulated insulin secretion in vivo. *bioRxiv* **2020**, 2020.04.22.055384.
72. Twig, G.; Elorza, A.; Molina, A. J.; Mohamed, H.; Wikstrom, J. D.; Walzer, G.; Stiles, L.; Haigh, S. E.; Katz, S.; Las, G.; Alroy, J.; Wu, M.; Py, B. F.; Yuan, J.; Deeney, J. T.; Corkey, B. E.; Shirihai, O. S., Fission and selective fusion govern mitochondrial segregation and elimination by autophagy. *EMBO J* **2008,** *27* (2), 433-46.
73. Ravassard, P.; Hazhouz, Y.; Pechberty, S.; Bricout-Neveu, E.; Armanet, M.; Czernichow, P.; Scharfmann, R., A genetically engineered human pancreatic β cell line exhibiting glucose-inducible insulin secretion. *J Clin Invest* **2011,** *121* (9), 3589-97.
74. Martinez-Sanchez, A.; Nguyen-Tu, M. S.; Leclerc, I.; Rutter, G. A., Manipulation and Measurement of AMPK Activity in Pancreatic Islets. *Methods Mol Biol* **2018,** *1732*, 413-431.
75. Hunter, R. W.; Foretz, M.; Bultot, L.; Fullerton, M. D.; Deak, M.; Ross, F. A.; Hawley, S. A.; Shpiro, N.; Viollet, B.; Barron, D.; Kemp, B. E.; Steinberg, G. R.; Hardie, D. G.; Sakamoto, K., Mechanism of action of compound-13: an α1-selective small molecule activator of AMPK. *Chem Biol* **2014,** *21* (7), 866-79.
76. Xiao, B.; Sanders, M. J.; Carmena, D.; Bright, N. J.; Haire, L. F.; Underwood, E.; Patel, B. R.; Heath, R. B.; Walker, P. A.; Hallen, S.; Giordanetto, F.; Martin, S. R.; Carling, D.; Gamblin, S. J., Structural basis of AMPK regulation by small molecule activators. *Nat Commun* **2013,** *4*, 3017.
77. Luo, J.; Deng, Z. L.; Luo, X.; Tang, N.; Song, W. X.; Chen, J.; Sharff, K. A.; Luu, H. H.; Haydon, R. C.; Kinzler, K. W.; Vogelstein, B.; He, T. C., A protocol for rapid generation of recombinant adenoviruses using the AdEasy system. *Nat Protoc* **2007,** *2* (5), 1236-47.
78. Agarwal, V.; Bell, G. W.; Nam, J. W.; Bartel, D. P., Predicting effective microRNA target sites in mammalian mRNAs. *Elife* **2015,** *4*.
79. Kozomara, A.; Griffiths-Jones, S., miRBase: annotating high confidence microRNAs using deep sequencing data. *Nucleic Acids Res* **2014,** *42* (Database issue), D68-73.
80. Chang, H.; Yi, B.; Ma, R.; Zhang, X.; Zhao, H.; Xi, Y., CRISPR/cas9, a novel genomic tool to knock down microRNA in vitro and in vivo. *Sci Rep* **2016,** *6*, 22312.
81. Patro, R.; Duggal, G.; Love, M. I.; Irizarry, R. A.; Kingsford, C., Salmon provides fast and bias-aware quantification of transcript expression. *Nat Methods* **2017,** *14* (4), 417-419.
82. Love, M. I.; Huber, W.; Anders, S., Moderated estimation of fold change and dispersion for RNA-seq data with DESeq2. *Genome Biol* **2014,** *15* (12), 550.
83. Shannon, P.; Markiel, A.; Ozier, O.; Baliga, N. S.; Wang, J. T.; Ramage, D.; Amin, N.; Schwikowski, B.; Ideker, T., Cytoscape: a software environment for integrated models of biomolecular interaction networks. *Genome Res* **2003,** *13* (11), 2498-504.
84. Martinez-Sanchez, A.; Nguyen-Tu, M. S.; Rutter, G. A., DICER Inactivation Identifies Pancreatic beta-Cell "Disallowed" Genes Targeted by MicroRNAs. *Mol Endocrinol* **2015,** *29* (7), 1067-79.
85. Jones, B.; Buenaventura, T.; Kanda, N.; Chabosseau, P.; Owen, B. M.; Scott, R.; Goldin, R.; Angkathunyakul, N.; Corrêa, I. R.; Bosco, D.; Johnson, P. R.; Piemonti, L.; Marchetti, P.; Shapiro, A. M. J.; Cochran, B. J.; Hanyaloglu, A. C.; Inoue, A.; Tan, T.; Rutter, G. A.; Tomas, A.; Bloom, S. R., Targeting GLP-1 receptor trafficking to improve agonist efficacy. *Nat Commun* **2018,** *9* (1), 1602.
86. Pasquier, A.; Vivot, K.; Erbs, E.; Spiegelhalter, C.; Zhang, Z.; Aubert, V.; Liu, Z.; Senkara, M.; Maillard, E.; Pinget, M.; Kerr-Conte, J.; Pattou, F.; Marciniak, G.; Ganzhorn, A.; Ronchi, P.; Schieber, N. L.; Schwab, Y.; Saftig, P.; Goginashvili, A.; Ricci, R., Lysosomal degradation of newly formed insulin granules contributes to β cell failure in diabetes. *Nat Commun* **2019,** *10* (1), 3312.
87. Ravier, M. A.; Rutter, G. A., Isolation and culture of mouse pancreatic islets for ex vivo imaging studies with trappable or recombinant fluorescent probes. *Methods Mol Biol* **2010,** *633*, 171-84.

88. Mitchell, R. K.; Nguyen-Tu, M. S.; Chabosseau, P.; Callingham, R. M.; Pullen, T. J.; Cheung, R.; Leclerc, I.; Hodson, D. J.; Rutter, G. A., The transcription factor. *J Biol Chem* **2017,** *292* (21), 8892-8906.
89. Wiemerslage, L.; Lee, D., Quantification of mitochondrial morphology in neurites of dopaminergic neurons using multiple parameters. *J Neurosci Methods* **2016,** *262*, 56-65.
90. Martinez-Sanchez, A.; Nguyen-Tu, M.-S.; Cebola, I.; Yavari, A.; Marchetti, P.; Piemonti, L.; de Koning, E.; Shapiro, A. M. J.; Johnson, P.; Sakamoto, K.; Smith, D. M.; Leclerc, I.; Ashrafian, H.; Ferrer, J.; Rutter, G. A., MiR-184 expression is regulated by AMPK in pancreatic islets.
91. Lu, T. T.; Heyne, S.; Dror, E.; Casas, E.; Leonhardt, L.; Boenke, T.; Yang, C. H.; Sagar; Arrigoni, L.; Dalgaard, K.; Teperino, R.; Enders, L.; Selvaraj, M.; Ruf, M.; Raja, S. J.; Xie, H.; Boenisch, U.; Orkin, S. H.; Lynn, F. C.; Hoffman, B. G.; Grün, D.; Vavouri, T.; Lempradl, A. M.; Pospisilik, J. A., The Polycomb-Dependent Epigenome Controls β Cell Dysfunction, Dedifferentiation, and Diabetes. *Cell Metab* **2018,** *27* (6), 1294-1308.e7.

FIGURE LEGENDS

Figure 1. Glucose stimulates islet miR-125b expression via AMPK repression. RT-qPCR measurements of **a-e,** MiR-125b in **a,** mouse and human islets cultured at the indicated glucose concentrations for 48h (**b**) human islets kept for 24h at 5.5mM glucose plotted agains donor's BMI, (**c**) islets from βAMPKdKO (green) and control (C, black) mice cultured at 5.5 or 25mM Glucose for 48h, (**d**) islets from βAMPKdKO (green), βLKB1KO (red) and control (C, black) male and female mice fed a chow or a ketogenic (Keto) diet for 28 days and (**e**) human islets treated with the AMPK activators C-13 and C-991 for 24h. **f,** Pri-miR-125b in isolated islets from βAMPKdKO (green) and littermate control (C, black) mice. Each dot represents islets from a single mouse or human donor. MiR-125b expression is normalized to that of the endogenous control miR-7d-3p[90] . ns= no significant, *p <0.05, **p <0.01, ***p <0.001, one-way ANOVA (repeated measures) and Dunnet multiple comparisons test (a), Pearson Correlation (b), two-way ANOVA (repeated measures) and Bonferroni multiple comparisons test (c), Student *t* test (d-f).

Figure 2. MiR-125b regulates insulin secretion in insulinoma/β-cell lines. Insulin content and Glucose-stimulated insulin secretion after 30 minutes of 17 or 15 mM glucose stimulation following overnight preincubation at 3 mM glucose. Data is presented as fold change of basal level. Each dot represent an independent experiment with three technical replicates. **a,** MIN6 cells were transfected with 5nM miR-125b or control mimics 48h before the experiment. **b,**

Experiments were performed with three different populations of CRISPR-mediated miR-125b KO and control cells. *p <0.05, paired Student t test.

Figure 3. High-through identification of miR-125b target genes. a, Schematic overview of the steps of the experimental approach used for the identification of miR-125b targets. MIN6 cells were transfected with control of miR-125b mimics. Then, total RNA was extracted, poly(A)-enriched and prepared for sequencing (n=5, T-RNA) or RNAs present in miRISC complexes were inmunoprecipitated with anti ago2-antibodies and submitted to RNA-seq (n=5, RIP-RNA). Differential analysis of gene expression was performed for both datasets separately generating fold change gene expression (miR-125b *vs* control) for all genes detected. Then both lists were combined to generate a ratio of Immunoprecipitated *vs* Total (poly(A) RNA). **b,** Enrichment of miR-125b seed sites in the 3'UTRs (left hand-side panel) and CDSs (right hand-side panel) of the mRNAs ranked according to RIP-RNA/T-RNA. The scatter plot shows the maxima of enrichment profile. Each dot represents a 7-letter word. The Y-position shows the maximum score of an enriched word and the X-position shows the gene-index where the Z-score is maximum. Top-ranked words with a left-shift associate with gene-expression change (lower gene index represents a stronger upregulation in RIP-RNA/T-RNA upon miR-125b transfection). The sequence of mature miR-125b is shown on the right, with the seed region in red. The reverse complementary sequence (RC) is also shown in red. **c)** Cytoscape-generated layout of genes with RIP-RNA/T-RNA ratio > 1.5 upon miR-125b overexpression. Node size represents the extent of the RIP-RNA/T-RNA ratio (the larger, the higher). The intensity of the gene node colour indicates the fold downregulation of each gene upon miR-125b expression (T-RNA). Downregulation at the transcript level was statistically significant for those genes represented in an octagonal shape. Lines connecting the nodes/genes with miR-125b indicate the presence of a predicted binding site for miR-125b as identified by TargetScan, with the intensity in the colour of the line representing the score (Total context score).

Figure 4. MiR-125b targets genes encoding mitochondrial and lysosomal proteins. a, Validation of miR-125b binding to the regions (full-length CDS or 3'UTR, as indicated) containing predicted miR-125b binding sites of six identified targets with highest RIP-RNA/T-RNA. Luciferase reporter assay of MIN6 cells cotransfected with pmirGLO plasmids containing the indicated target downstream the luciferase ORF and miR-125b (+) or non-targeting (-) control mimics. Samples were measured 24h after transfection in technical replicates. *Firefly* luciferase values are normalised to *Renilla*'s, independently expressed by the same vector and are shown as relative to that obtained for each construct cotransfected with the control miRNA mimic. Each dot represents and independent experiment. A construct containing three perfectly complementary binding sites for miR-125b (positive control) and the empty pmiRGlo vector (negative control) were included in the experiments. **b,** Gene Ontology enrichment analysis of the genes significanty up- and down-regulated upon miR-125b overexpression (T-RNA) and putative miR-125b direct targets (RIP-RNA/T-RNA > 1.5) performed with DAVID. The graph shows enrichment scores for one representative term for each cluster grouped by semantic similarities and including terms with a padj (Benjamini) < 0.05. See Supp Table 2 for a full list of terms. *p <0.05, ***p < 0.001, ****p<0.0001, Student t test values of the log[fold change] values.

Figure 5. MiR-125b represses *M6PR* and alters lysosomal morphology. a, MIN6 cells were transfected with luciferase reporters containing the M6pr 3'UTR with (mutated, MUT) or without (wild-type, WT) three point mutations in the sequence complementary to the miR-125b seed. Control (-) or miR-125b (+) mimics were co-transfected and *Firefly* luciferase values normalized to *Renilla*'s. Each dot represents and independent experiment. **b,** Representative Western blot showing reduced (left-hand side panel) and increased (right hand-side panel) M6PR protein levels upon miR-125b overexpression or CRISPR-Cas9-mediated deletion of miR-125b in EndoCβ-H1 cells, respectively. Bar graphs show densitometry quantification of M6PR, using ImageJ, normalized by tubulin and presented relative to the control. **c,** Left hand-side panel: RT-qPCR measurement of *M6PR* mRNA in EndoCβ-H1 cells transfected with

control (C) or miR-125b (125b) mimics, normalized by the housekeeping gene *Ppia* and presented as fold change of the control. Right hand-side panel: Normalized (Reads *per* Kilobase of transcript, *per* Million mapped reads (RPKM)) M6PR reads in Control *vs* MIR125B2-KO (KO) EndoCβ-H1 cells. **d,** Representative Transmission Electron Microscopy image of MIN6 cells transfected for 48h with control (C) or miR-125b (125B) mimics. Red arrows show enlarged lysosomal structures. Scale bar = 1 µm. These were not observed in any of the imaged controls (n=3 independent experiments). *p <0.05, ***p < 0.001, ****p<0.0001, Student t test of the log[fold change] values.

Figure 6. MiR-125b represses *MTFP1* and alters mitochondria morphology. a, MIN6 cells were transfected with luciferase reporters containing the *Mtfp1* 3'UTR with (mutated, MUT) or without (wild-type, WT) two point mutations in the sequence complementary to the miR-125b seed. Control (-) or miR-125b (+) mimics were co-transfected and *Firefly* luciferase values normalized to *Renilla*'s. Each dot represents and independent experiment. **b,c,** Quantitative analysis of mitochondria number and morphology on deconvoluted confocal images of (B) MIN6 cells transfected with miR-125b (red) or control (black) mimics or (C) EndoCβ-H1 with CRISPR/Cas9-mediated miR-125b deletion (green) or controls (black). Cells were stained with Mitotracker green. An ImageJ macro was generated and used to quantify number of mitochondria per cell, total mitochondria area, individual mitochondria length (elongation), circularity (0:elongated; 1:circular) and perimeter. Each dot represents one acquisition (n=3 (B), n=4 (C) independent experiments). Lower panels show representative confocal images of the mitochondrial network of EndoCβ-H1-MIR125B2-KO and control cells. Scale bar: 10 µm. *p <0.05, **p<0.01, ***p < 0.001, ****p<0.0001, Student t test values of the log[fold change] values (a); Student t test (b, c).

Figure 7. Mice with β-cell-selective overexpression of miR-125b are glucose intolerant and present impaired glucose stimulated insulin secretion. a, MiR-125b RT-qPCR in isolated islets from Control (RIP7-rtTA$^{+/-}$) and MIR125B-Tg mice (RIP7-rtTA$^{+/-}$, MIR125B Tg$^{+/-}$). Data are fold change *vs* Control. **b,** Glycaemia in 5 and 9 week old Control and MiR125B-

Tg mice fed *ad libitum*. For A and B, each dot represents a single mouse. **c, d,** Glucose tolerance test in 6 and 10 week old MIR125B-Tg and littermate control male (C) and female (D) mice. n=7-8C, 5-7Tg. **e,** Glucose (3 g/kg)-induced insulin secretion assessed in 10 week old MIR125B-Tg and littermate controls (n=13C, 11 Tg). **f,** Pancreata from MIR125B-Tg and littermate controls were fixed and subjected to immunocytochemical analysis for insulin and glucagon. β- and α-cell masses are presented as the β-cell/α-cell ratio and correspond to quantification of insulin-positive area/glucagon positive area ratio (left-hand side panel). β-Cell mass is presented as a percentage of the pancreatic surface and corresponds to quantification of the insulin-positive area per pancreas area quantified in whole pancreas sections. Each dot represents one pancreatic section with n = 3 mice/genotype. *p <0.05, **p<0.01, ***p < 0.001, ****p<0.0001, Student t test (a, b, f); two-way ANOVA (repeated-measures), Fisher least significance different test (c-e).

Figure 8. MIR125B-Tg islets contain and secrete less insulin than controls. a, Insulin secretion in response to 30 minutes low (3mM, LG) or high (17mM, HG) glucose or KCl (17mM KCl and 3mM Glucose) in islets from 10-11 week old Control (RIP7-rtTA$^{+/-}$) and MIR125B-Tg (RIP7-rtTA$^{+/-}$, MIR125B Tg$^{+/-}$) mice (left hand-side panel). The right hand-side panel shows fold induction *vs* low glucose. **b,c,** Insulin and pro-insulin content in 10 week old Control (C) and MIR125B-Tg (Tg) mice quantified by HTRF (B) and Western blot (WB, C). A representative WB is shown with islets from 3 C and 3 Tg animals. Bar graphs show densitometry quantification of insulin and pro-insulin, using ImageJ, normalized by GAPDH and presented relative to the average control. **d)** ATP rises in response to high glucose (17mM *vs* 3mM) and **e,** ATP/ADP ratio at 3mM glucose in intact MIR125B-Tg and control islets infected with an adenoviral Perceval sensor. n=4-5 mice/genotype, with 1-2 acquisitions per mouse and an average of 5 islets/acquisition. **f,** Ca^{2+} rises in response to high glucose (17mM *vs* 3mM) and KCl (20mM KCl, 3mM Glucose) in intact MIR125B-Tg and control islets incubated with Cal-520. n=4-5 mice/genotype, with 1-2 acquisitions per mouse and an average of 5 islets/acquisition. For (D) and (F), AUC corresponding to HG incubation were

determined and presented on the right. **g,** NP-Y.Venus fluorescence increases in response to 20mM KCl in cells from dissociated MIR125B-Tg and control islets infected with an adenoviral NP-Y-venus sensor. n=3-4C mice/genotype 2ith 2 acquisitions per mouse and 1-2 β-cells per acquisition. In all graphs, each dot represents a single mouse. ns=not significant *p <0.05, **p<0.01, ***p < 0.001, two-way ANOVA (repeated-measures) and Bonferroni multiple comparisons test (a), Student t test (b-f).

Figure 9. Enlarged lysosomes/autophagolysosomes are abundant in miR-125b transgenic islets. a, Quantitative analysis of mitochondria number and morphology on deconvoluted confocal images of dissociated MIR125B-Tg and Control islets from 10-11 week old mice. Cells were stained with Mitotracker green. An ImageJ macro was generated and used to quantify number of mitochondria per cell, total mitochondria area, individual mitochondria length (elongation), circularity (0:elongated; 1:circular) and perimeter. Each dot represents one cell (n=3 mice/genotype). **b,** Mitochondrial DNA copy number, calculated as the ratio of the mitochondrial encoded gene mt-Nd1 to the nuclear Cxcl12. Each dot represents a single mouse. **c,** Representative Transmission Electron Microscopy images of MIR125B-Tg and control β-cells. Red arrows: enlarged lysosomes with undigested cargos. Blue arrows: non-crystalized insulin granules, showing a rod like structure or a grey interior. Scale bar = 1µm, 40nm (bottom right) interior. **d,** Number of enlarged lysosomes per field imaged. **e,** β-cell granule density. For (D-E) each dot represents one image (n=3 mice/genotype, 9-13 images/mouse). *p <0.05, **p<0.01, ****p < 0.0001, Student t test.

Figure 10. MiR125b overexpression alters gene expression in mouse and human islets. a, Gene Ontology analysis of significantly (padj <0.1) down-regulated (left, red) and up-regulated genes (right, green) in MIR125B-Tg islets from 6-week old mice *vs* controls performed with DAVID. The graph shows enrichment scores for one representative term for each cluster grouped by semantic similarities and including terms with padj (Benjamini) < 0.05. See Supp Table 6 for a full list of terms. **b,** KEGG pathway “Insulin secretion”. Red and blue stars indicate significantly down- and up-regulated genes in MIR125B-Tg islets *vs* control,

respectively. *Sytl4* (granuphilin) has been manually added to the pathway. **c,** Gene Set Enrichment Analysis (GSEA) of genes ranked by fold change in human islets infected with an adenovirus expressing miR-125 *vs* control during 24h. The graph shows enrichment scores for significantly ($p<0.05$) down- (red, top plot) and up-regulated (green, bottom plot) KEGG pathways terms. See Supp Table 8 for a full list of terms. Examples of enrichment plots (Lysosome and calcium signalling KEGG pathways) are shown in **d**.

Table 1. MiR-125b direct targets identified by integration of RIP-seq and T-RNA-seq differential analysis. Genes (182) with RIP-seq to T-RNA ratio > 1.5 are shown. FoldC_T-RNA and padj_T-RNA= Fold change and adjusted p-value of differential analysis of transcripts in MIN6 cells transfected with miR-125b mimics vs controls. FoldC_RIP and padj_RIP= Fold change and adjusted p-value of differential analysis of Ago2-immunoprecipitated RNAs in MIN6 cells transfected with miR-125b mimics vs controls. Predicted binding site TargetScan=Y indicates the presence of at least one predicted miR-125b binding site by TargetScan mouse v7.2.

Supplemental Figure 1. Human islet miR-125b expression does not correlated with age or sex of the donors. RT-qPCR measurements of miR-125b human islets cultured at 5.5mM glucose plotted against islet donor age (**a**) or sex (**b**). Each dot represents islets from a single human donor. MiR-125b expression is normalized to that of the endogenous control miR-7d-3p[90] . Pearson Correlation (a).

Supplemental Figure 2. Chromatin accessibility of *MIR125B1/2* in mouse islets. Integration of ATAC-seq enrichment profiles in βLKB1KO (red) and control (black) islets with SLIC-CAGE-determined TSS in control islets and with published datasets of ChIP-seq data of histone modifications (H3K4me3, blue) in mouse islets [91] and Smad2/3 (Orange)in pancreatic ductal adenocarcinoma cells (PDAC)[17] in the *MIR125B-1* (**a**) and *MIR125B-2* (**b**) loci. Red arrow indicates an ATAC-seq significantly more accessible (more open) in βLKB1KO islets *vs* controls. Genecode VM23 transcript set is shown in dark blue. Alignment with the human DNA track is presented in black.

Supplemental Figure 3. RT-qPCR measurements of *Smad2* (**a**) and *Smad3*(**b**) mRNAs and miR-125b-5p **(c)** in MIN6 cells 48h after the transfection of Smad2, Smad3 or control siRNAs. Each dot represents an independent experiment. Values were normalized by the endogenous control *Ppia* (cyclophilin a, (a,b) or let-7d-3p (c) and are presented as fold change relative to control siRNA. ***p <0.001, ***p<0.0001, Student t test of the log[fold change] values.

Supplemental Figure 4. Elimination of miR-125b by CRISPR-Cas9 in EndoCβ-H1 cells. a, Schematic representation of the targeting location of the gRNAs in *MIR125B-1* and *MIR125B-2* human loci. Two independent pairs of gRNAs were designed for each loci, targeting the seed of miR-125b (miR-125b-5p) or the regions essential for DROSHA and/or DICER cleavage. **b,** RT-qPCR measurements of (mature) miR-125b in Control EndoCβ-H1 (containing the RIP-Cas9 vector, but no gRNAs), MIR125B1-KO1 and MIR125B1-KO2 (containing RIP-Cas9 vector with gRNAs targeting the *MIR125B1* locus, pair 1 (KO1) or pair 2(KO2)), MIR125B2-KO1 and MIR125B2-KO2 (containing RIP-Cas9 vector with gRNAs targeting the *MIR125B2* locus, pair 1 (KO1) or pair 2(KO2)) or combinations of the above gRNAs as indicated. **c,** RT-qPCR of miR-99a and miR-125a in Control (C) and MIR125B2-KO1 (KO) cells. Each dot represents an independent experiment. Values were normalized by the endogenous control let-7d-3p and are presented as fold change relative to control cells. ns=not significant, **p<0.01, ***p <0.001, ***p<0.0001, Student t test of the log[fold change] values.

Supplemental Figure 5. β-cell-selective overexpression of miR-125b does not alter hypothalamic miR-125b expression, body weight, insulin tolerance and β-cell growth and apoptosis. a, RT-qPCR of miR-125b in hypothalamus from Control (RIP7-rtTA$^{+/-}$) and MIR125B-Tg mice (RIP7-rtTA$^{+/-}$, MIR125B Tg$^{+/-}$). **b,** Body weight of male and female MIR125B-Tg and littermate control mice monitored weekly from the age of 5 weeks. n=5-8 mice/genotype. **c,** Glucose tolerance test in 6 week old mice containing the transgene in the absence of rtTA (-rtTA Control, MIR125B Tg$^{+/-}$) and littermate controls without the transgene or rtTA, showing that the presence of the transgene doesn't affect glucose tolerance. n=4-6

mice/genotype. **d,** Intraperitoneal Insulin tolerance test in 7 week old MIR125B-Tg and littermate control male and female mice. n=5-8 mice/genotype. **e,f,** Pancreata from 11 week-old MIR125B-Tg and littermate controls were fixed and subjected to (E) immunocytochemical analysis for insulin and Ki67. The number of Ki67-positive cells is expressed as a percentage of insulin-positive cells (F) TUNEL assay for *in situ* detection of apoptotic cells. The number of TUNEL-positive cells is presented as a percentage of insulin-positive cells. Each dot represents one pancreatic section with n=3 mice/genotype. **g,** Quantitative analysis of lysosomes number and total area on deconvoluted confocal images of dissociated MIR125B-Tg and Control islets from 10-11 week old mice. Cells were stained with Lysotracker green. An ImageJ macro was generated and used to quantify number of lysosomes per cell and total lysosomal area. Each dot represents one cell (n=3 mice/genotype). ns=not significant, *p <0.05, ***p < 0.001, ****p<0.0001, Student t test (a, e-g), two-way ANOVA (repeated-measures), Fisher least significance different test (b-d)

Supplemental Figure 6. Overexpression of miR-125b in human islets. a, RT-qPCR of miR-125b in dissociated human islets 24h hours following infection with 2 MOI of an adenovirus expressing miR-125b (pAd-MIR125B) or control (pAd-empty). **b,** Principal Component Analysis of the RNA-seq data in human dissociated islets infected with pAd-MIR125B or control (C) adenovirus. HI=Human islets. 3 independent experiments were performed with islets from three different donors (H1-3). ***p<0.0001, Student t test of the log[fold change] values.

Graphical abstract

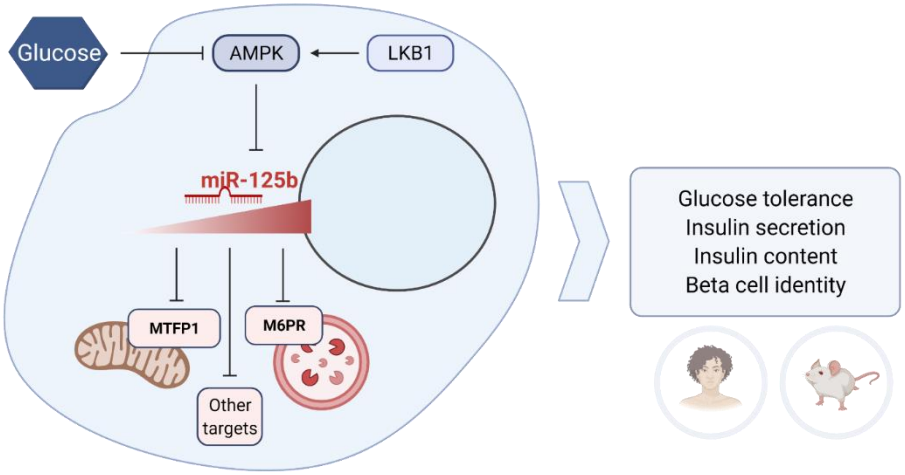

Figure 1

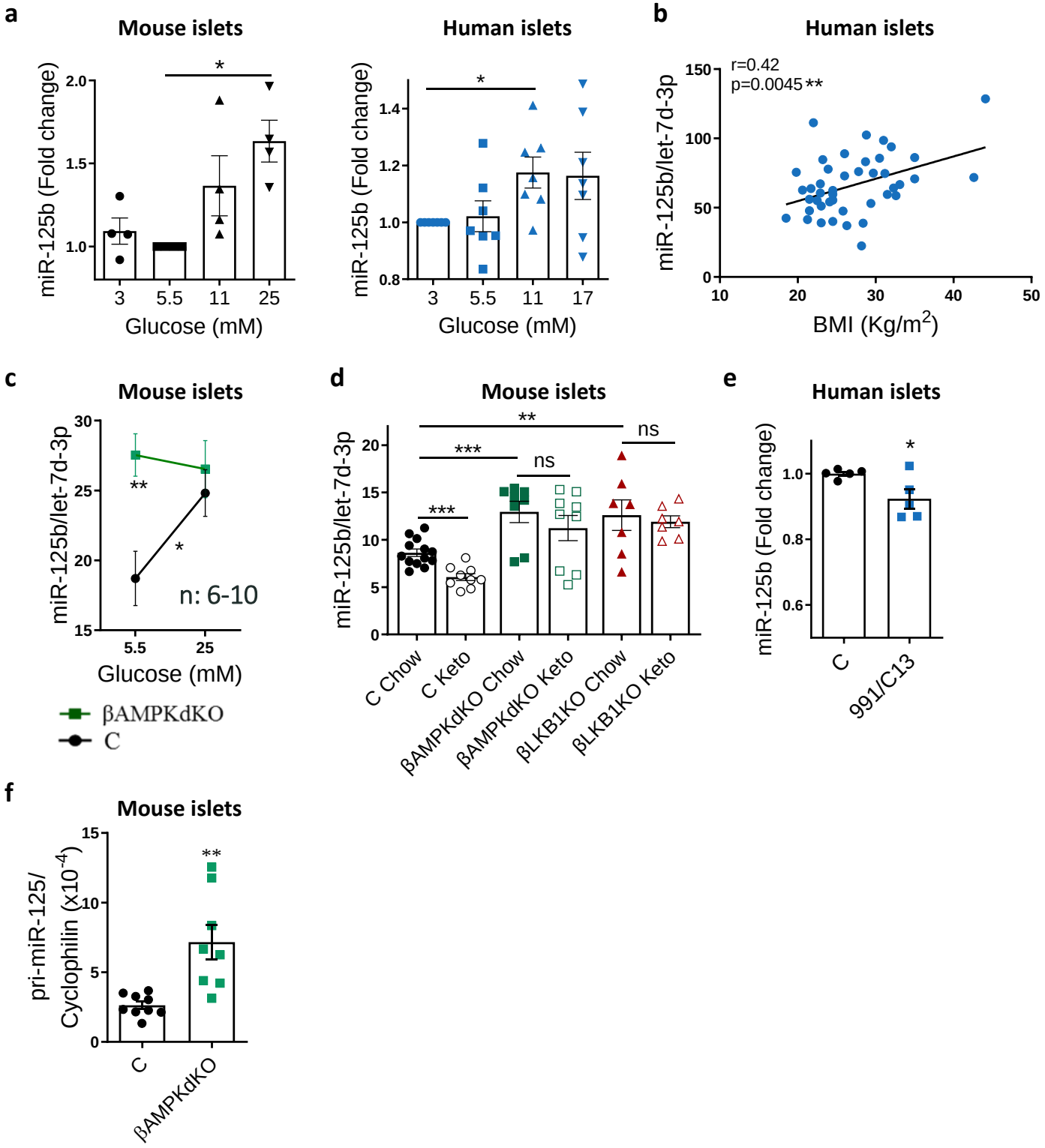
a
Mouse islets
miR-125b (Fold change)
2.0
1.5
1.0
*
3
5.5
11
25
Glucose (mM)
Human islets
miR-125b (Fold change)
1.4
1.2
1.0
0.8
*
3
5.5
11
17
Glucose (mM)
b
Human islets
r=0.42
p=0.0045 **
miR-125b/let-7d-3p
150
100
50
0
10
20
30
40
50
BMI (Kg/m2)
c
Mouse islets
miR-125b/let-7d-3p
30
25
20
15
**
*
n: 6-10
5.5
25
Glucose (mM)
βAMPKdKO
C
d
Mouse islets
miR-125b/let-7d-3p
20
15
10
5
0
**
ns
***
ns
***
C Chow
C Keto
βAMPKdKO Chow
βAMPKdKO Keto
βLKB1KO Chow
βLKB1KO Keto
e
Human islets
miR-125b (Fold change)
1.0
0.8
0.6
*
C
991/C13
f
Mouse islets
pri-miR-125/
Cyclophilin (x10-4)
15
10
5
0
**
C
βAMPKdKO

Figure 2

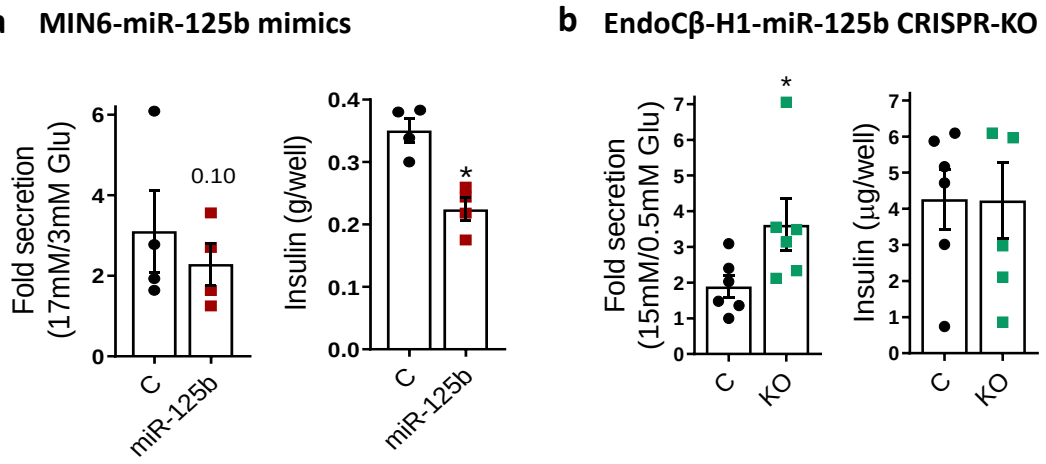
a
MIN6-miR-125b mimics
Fold secretion (17mM/3mM Glu)
0.10
C
miR-125b
Insulin (g/well)
*
b
EndoCβ-H1-miR-125b CRISPR-KO
Fold secretion (15mM/0.5mM Glu)
*
C
KO
Insulin (µg/well)

Figure 3

a

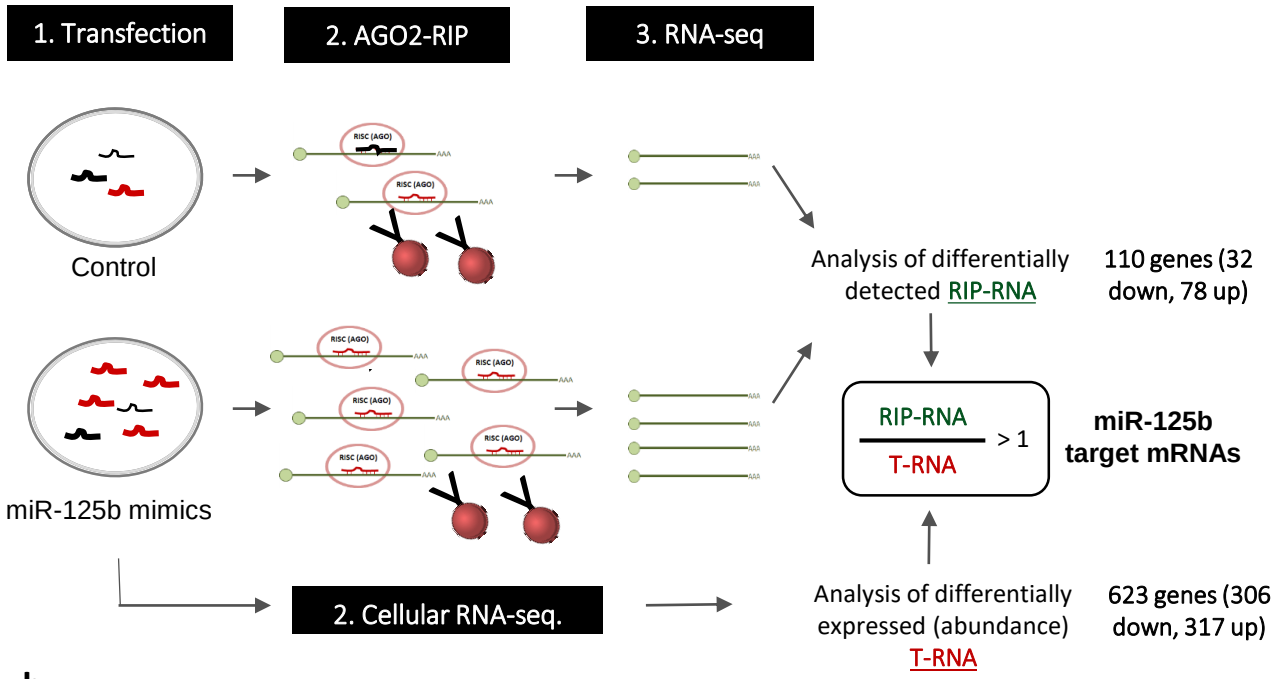

b

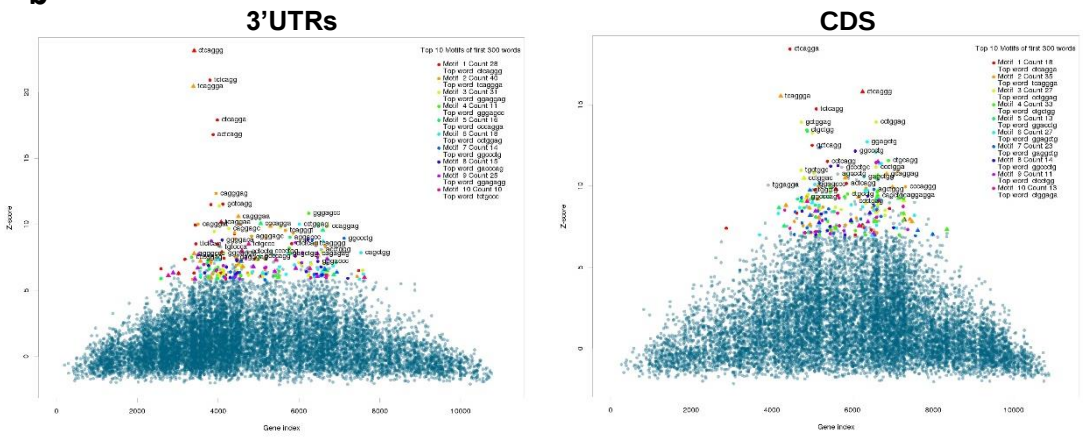

>mmu-miR-125b-5p
UCCCUGAGACCCUAA
CUUGUGA

RC: TCTCAGGGA

c

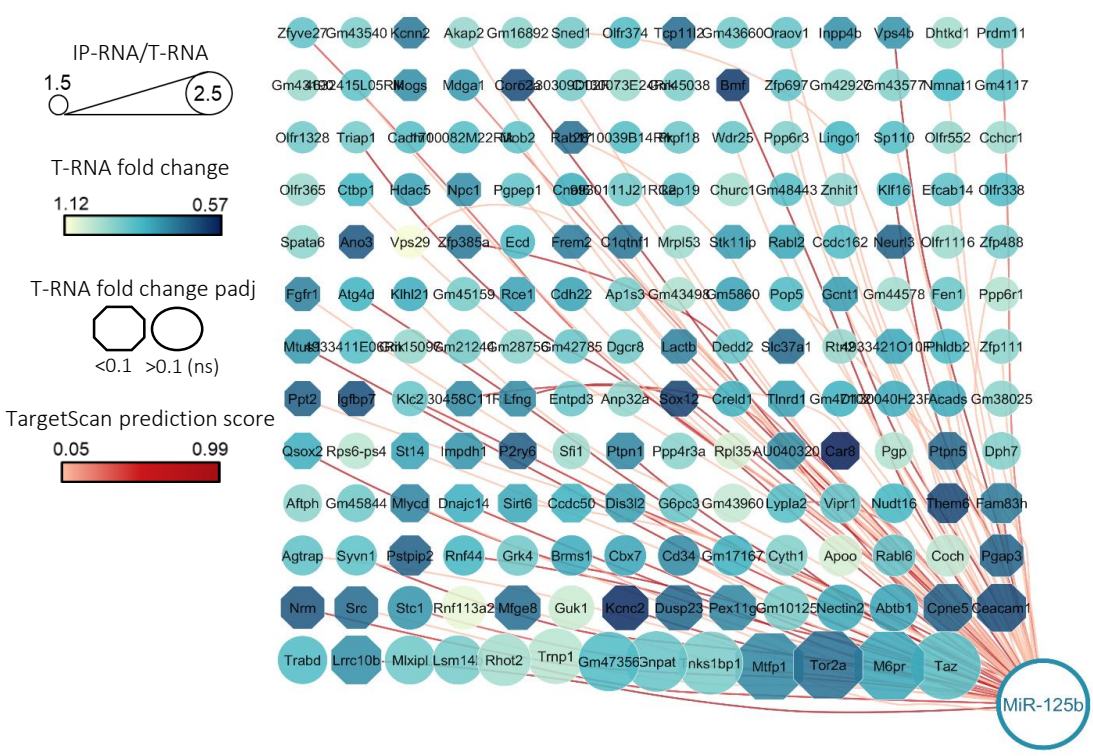

Table 1

Gene.name	Predicted binding site TargetScan	FoldC_T-RNA	padj_T-RNA	FoldC_RIP	padj_RIP	RIP/T-RNA
Taz	Y	0.88	0.213	2.196	0	2.494
M6pr	Y	0.818	0.006	2.039	0	2.494
Tor2a	Y	0.722	0.002	1.786	0	2.476
Mtfp1	Y	0.762	0.018	1.865	0	2.449
Tnks1bp1		0.927	0.607	2.194	0	2.366
Gnpat		0.901	0.44	2.067	0	2.294
Gm47356		0.869	0.602	1.965	0.002	2.262
Trnp1		1.018	0.968	2.201	0	2.163
Rhot2	Y	0.992	0.982	2.051	0	2.068
Lsm14b		0.924	0.611	1.833	0	1.985
Mlxipl		0.915	0.743	1.812	0	1.981
Lrrc10b	Y	0.774	0.029	1.521	0.056	1.966
Trabd		0.867	0.416	1.697	0.001	1.957
Ceacam1	Y	0.66	0.002	1.284	0.608	1.944
Cpne5	Y	0.694	0.016	1.345	0.613	1.937
Abtb1	Y	0.814	0.242	1.576	0.025	1.935
Nectin2		0.821	0.114	1.572	0.05	1.915
Gm10125		0.925	0.818	1.745	0.03	1.886
Pex11g		0.756	0.06	1.419	0.486	1.876
Dusp23	Y	0.703	0.006	1.319	0.768	1.875
Kcnc2	Y	0.6	0	1.118	0.999	1.864
Guk1		1.045	0.896	1.944	0	1.86
Mfge8	Y	0.712	0.013	1.32	0.771	1.853
Rnf113a2		1.088	0.494	1.998	0.001	1.836
Stc1	Y	0.785	0.142	1.44	0.406	1.833
Src	Y	0.712	0.011	1.285	0.852	1.804
Nrm	Y	0.674	0	1.214	0.963	1.801
Pgap3	Y	0.698	0	1.257	0.802	1.801
Coch		1.027	0.954	1.849	0.004	1.8
Rabl6	Y	0.891	0.331	1.591	0.001	1.786
Apoo		1.059	0.689	1.886	0.004	1.781
Cyth1	Y	0.94	0.514	1.658	0.001	1.763
Gm17167		0.84	0.445	1.478	0.364	1.758
Cd34	Y	0.764	0.123	1.34	0.662	1.753
Cbx7	Y	0.817	0.13	1.431	0.379	1.753
Brms1	Y	0.826	0.11	1.446	0.428	1.75
Grk4		0.914	0.787	1.597	0.175	1.746
Rnf44	Y	0.849	0.338	1.478	0.025	1.741
Pstpip2		0.691	0.002	1.203	0.999	1.74
Syvn1	Y	0.886	0.393	1.54	0	1.738
Agtrap	Y	0.891	0.601	1.547	0.258	1.737
Fam83h	Y	0.738	0.001	1.278	0.543	1.732
Them6	Y	0.649	0.001	1.123	0.999	1.731
Nudt16		0.849	0.234	1.467	0.402	1.728
Vipr1	Y	0.893	0.499	1.541	0	1.726
Lypla2	Y	0.874	0.204	1.501	0.037	1.718
Gm43960		1.035	0.938	1.767	0.029	1.707
G6pc3		0.9	0.517	1.532	0.114	1.703
Dis3l2	Y	0.805	0.012	1.367	0.64	1.699
Ccdc50		0.841	0.073	1.429	0.233	1.698
Sirt6	Y	0.82	0.019	1.386	0.607	1.692
Dnajc14	Y	0.834	0.002	1.403	0.329	1.683
Mlycd	Y	0.754	0.002	1.267	0.775	1.681
Gm45844		0.913	0.75	1.53	0.196	1.676
Aftph		0.956	0.747	1.597	0.018	1.671
Dph7		0.941	0.774	1.571	0.209	1.669
Ptpn5		0.706	0.011	1.176	0.999	1.666
Pgp	Y	1.01	0.98	1.682	0.004	1.665
Car8		0.58	0	0.965	0.999	1.664
AU040320	Y	0.769	0	1.274	0.533	1.656
Rpl35		1.06	0.839	1.75	0.003	1.651
Ppp4r3a	Y	0.95	0.789	1.564	0.003	1.646
Ptpn1	Y	0.759	0	1.248	0.805	1.645
Sfi1		0.984	0.954	1.615	0.146	1.642
P2ry6		0.687	0	1.127	0.999	1.641
Impdh1		0.785	0.003	1.286	0.379	1.639
St14	Y	0.811	0.087	1.327	0.752	1.636
Rps6-ps4		1.021	0.957	1.668	0.078	1.633
Qsox2	Y	0.832	0.026	1.357	0.096	1.632
Gm38025		0.957	0.89	1.561	0.243	1.631
Acads	Y	0.823	0.183	1.342	0.441	1.629
D130040H23Rik	Y	0.828	0.28	1.348	0.673	1.628
Gm47102		0.837	0.442	1.361	0.428	1.626
Tlnrd1		0.809	0.097	1.315	0.533	1.626
Creld1	Y	0.838	0.189	1.36	0.517	1.623
Sox12	Y	0.639	0	1.036	0.999	1.622
Anp32a		0.963	0.908	1.559	0.006	1.619
Entpd3	Y	0.903	0.604	1.456	0.078	1.613
Lfng	Y	0.767	0.075	1.236	0.845	1.613
6030458C11Rik	Y	0.764	0	1.228	0.684	1.608
Klc2	Y	0.903	0.536	1.45	0.11	1.606
Igfbp7		0.66	0.002	1.059	0.999	1.604
Ppt2	Y	0.69	0	1.106	0.999	1.603
Zfp111	Y	0.958	0.842	1.534	0.111	1.601
Phldb2	Y	0.86	0.455	1.377	0.375	1.6
4933421O10Rik		0.818	0.035	1.307	0.8	1.598
Rtn2		0.966	0.896	1.544	0.037	1.597
Slc37a1		0.702	0	1.12	0.999	1.596
Dedd2		0.899	0.682	1.431	0.286	1.592

Table 1-cont

Gene.name	Predicted binding site TargetScan	FoldC_T-RNA	padj_T-RNA	FoldC_RIP	padj_RIP	RIP/T-RNA
Lactb	Y	0.751	0.027	1.195	0.999	1.59
Dgcr8		0.917	0.618	1.459	0.375	1.59
Gm42785		0.902	0.612	1.433	0.379	1.589
Gm28756		0.955	0.912	1.515	0.303	1.587
Gm21244		0.917	0.763	1.455	0.39	1.587
Gm15097		0.967	0.939	1.535	0.258	1.586
4933411E06Rik		0.876	0.62	1.389	0.502	1.585
Mtus1	Y	0.794	0.052	1.259	0.917	1.584
Ppp6r1		1.011	0.96	1.601	0.001	1.584
Fen1		0.906	0.534	1.434	0.072	1.583
Gm44578		0.989	0.984	1.564	0.229	1.582
Gcnt1	Y	0.799	0.044	1.263	0.501	1.581
Pop5	Y	0.867	0.448	1.37	0.243	1.581
Gm5860		0.81	0.262	1.278	0.828	1.579
Gm43498		1.005	0.994	1.585	0.183	1.578
Ap1s3	Y	0.927	0.705	1.462	0.39	1.577
Cdh22	Y	0.808	0.18	1.274	0.666	1.576
Rce1		0.809	0.081	1.275	0.69	1.576
Gm45159		0.926	0.82	1.459	0.398	1.576
Klhl21	Y	0.829	0.286	1.306	0.693	1.576
Atg4d	Y	0.843	0.405	1.329	0.613	1.576
Fgfr1	Y	0.747	0.012	1.175	0.999	1.574
Zfp488	Y	0.924	0.734	1.454	0.428	1.574
Olfr1116		0.982	0.969	1.543	0.258	1.572
Neurl3		0.691	0.005	1.086	0.999	1.571
Ccdc162		0.869	0.499	1.365	0.582	1.57
Rabl2	Y	0.82	0.098	1.287	0.878	1.569
Stk11ip		0.801	0.002	1.255	0.9	1.568
Mrpl53		0.981	0.958	1.538	0.105	1.567
C1qtnf1	Y	0.729	0.024	1.143	0.999	1.567
Frem2		0.739	0.05	1.159	0.999	1.567
Ecd		0.859	0.153	1.346	0.49	1.567
Zfp385a	Y	0.735	0.01	1.15	0.999	1.565
Vps29	Y	1.106	0.536	1.73	0.001	1.564
Ano3		0.673	0.008	1.053	0.999	1.564
Spata6		0.958	0.869	1.494	0.358	1.56
Olfr338		0.866	0.549	1.35	0.603	1.559
Efcab14	Y	0.887	0.301	1.382	0.364	1.559
Klf16	Y	0.863	0.152	1.345	0.594	1.559
Znhit1	Y	0.959	0.885	1.492	0.353	1.556
Gm48443		0.875	0.404	1.361	0.533	1.556
Churc1		0.993	0.986	1.545	0.234	1.555
Cep19		0.899	0.523	1.397	0.533	1.554
9930111J21Rik2	Y	0.914	0.785	1.421	0.375	1.554
Cnot6		0.83	0.168	1.289	0.144	1.553
Pgpep1	Y	0.894	0.61	1.384	0.385	1.548
Npc1		0.771	0.001	1.193	0.977	1.547
Hdac5		0.809	0.151	1.25	0.942	1.544
Ctbp1	Y	0.848	0.005	1.303	0.43	1.537
Olfr365		0.979	0.954	1.505	0.353	1.537
Cchcr1		0.981	0.936	1.507	0.328	1.536
Olfr552		0.967	0.94	1.485	0.345	1.536
Sp110		0.871	0.609	1.337	0.648	1.535
Lingo1	Y	0.852	0.312	1.308	0.474	1.535
Ppp6r3	Y	0.939	0.618	1.438	0.023	1.531
Wdr25	Y	0.9	0.551	1.377	0.533	1.53
Prpf18		0.907	0.322	1.386	0.443	1.528
2810039B14Rik		0.871	0.496	1.33	0.708	1.528
Rab17	Y	0.718	0.005	1.097	0.999	1.528
Mob2	Y	0.889	0.391	1.355	0.486	1.525
1700082M22Rik		0.874	0.62	1.333	0.717	1.525
Cadm1		0.872	0.385	1.33	0.366	1.525
Triap1	Y	0.923	0.687	1.408	0.382	1.524
Olfr1328		0.915	0.715	1.394	0.366	1.523
Gm4117		0.878	0.609	1.337	0.639	1.523
Nmnat1	Y	0.852	0.408	1.297	0.819	1.523
Gm43577		0.94	0.864	1.431	0.465	1.523
Gm42927		0.972	0.941	1.479	0.328	1.522
Zfp697	Y	0.888	0.597	1.35	0.689	1.519
Bmf	Y	0.623	0	0.946	0.999	1.519
Gm45038		0.93	0.795	1.412	0.401	1.518
C130073E24Rik		0.979	0.963	1.487	0.36	1.518
E130309D02Rik	Y	0.924	0.716	1.4	0.366	1.516
Coro2a	Y	0.656	0	0.994	0.999	1.514
Mdga1	Y	0.794	0.193	1.201	0.999	1.513
Mogs		0.772	0.05	1.167	0.857	1.512
4632415L05Rik	Y	0.886	0.414	1.339	0.713	1.511
Gm43190		0.978	0.96	1.477	0.375	1.511
Prdm11	Y	0.907	0.683	1.369	0.648	1.51
Dhtkd1		0.991	0.986	1.496	0.345	1.509
Vps4b	Y	0.784	0.053	1.183	0.999	1.509
Inpp4b		0.779	0.076	1.174	0.999	1.508
Oraov1	Y	0.898	0.369	1.354	0.637	1.508
Gm43660		0.916	0.76	1.382	0.419	1.508
Tcp11l2		0.711	0.019	1.072	0.999	1.508
Olfr374		0.87	0.551	1.31	0.786	1.506
Sned1	Y	0.921	0.808	1.387	0.348	1.505
Gm16892		0.958	0.925	1.441	0.375	1.504
Akap2	Y	0.97	0.944	1.458	0.286	1.502
Kcnn2		0.734	0.052	1.102	0.999	1.501

Figure 4

a

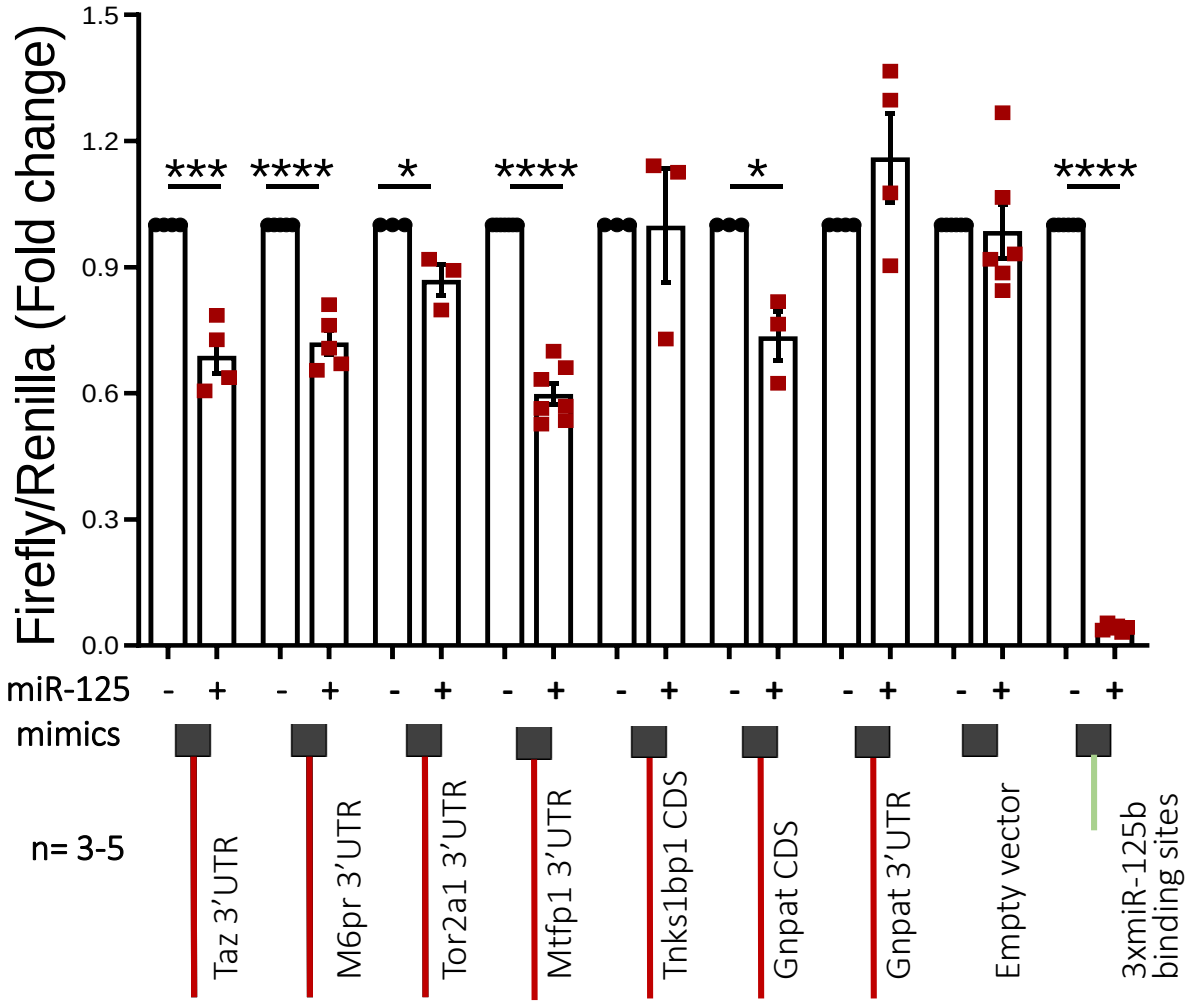
Firefly/Renilla (Fold change)
1.5
1.2
0.9
0.6
0.3
0.0
***
****
*
****
*
****
miR-125
mimics
n= 3-5
Taz 3'UTR
M6pr 3'UTR
Tor2a1 3'UTR
Mtfp1 3'UTR
Tnks1bp1 CDS
Gnpat CDS
Gnpat 3'UTR
Empty vector
3xmiR-125b binding sites

b

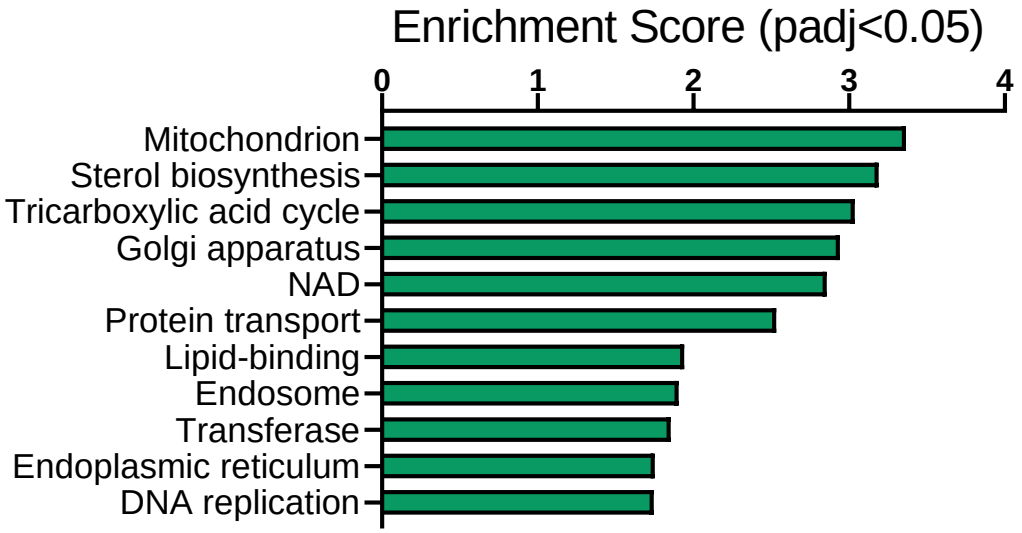
Enrichment Score (padj<0.05)
0
1
2
3
4
Mitochondrion
Sterol biosynthesis
Tricarboxylic acid cycle
Golgi apparatus
NAD
Protein transport
Lipid-binding
Endosome
Transferase
Endoplasmic reticulum
DNA replication

Figure 5

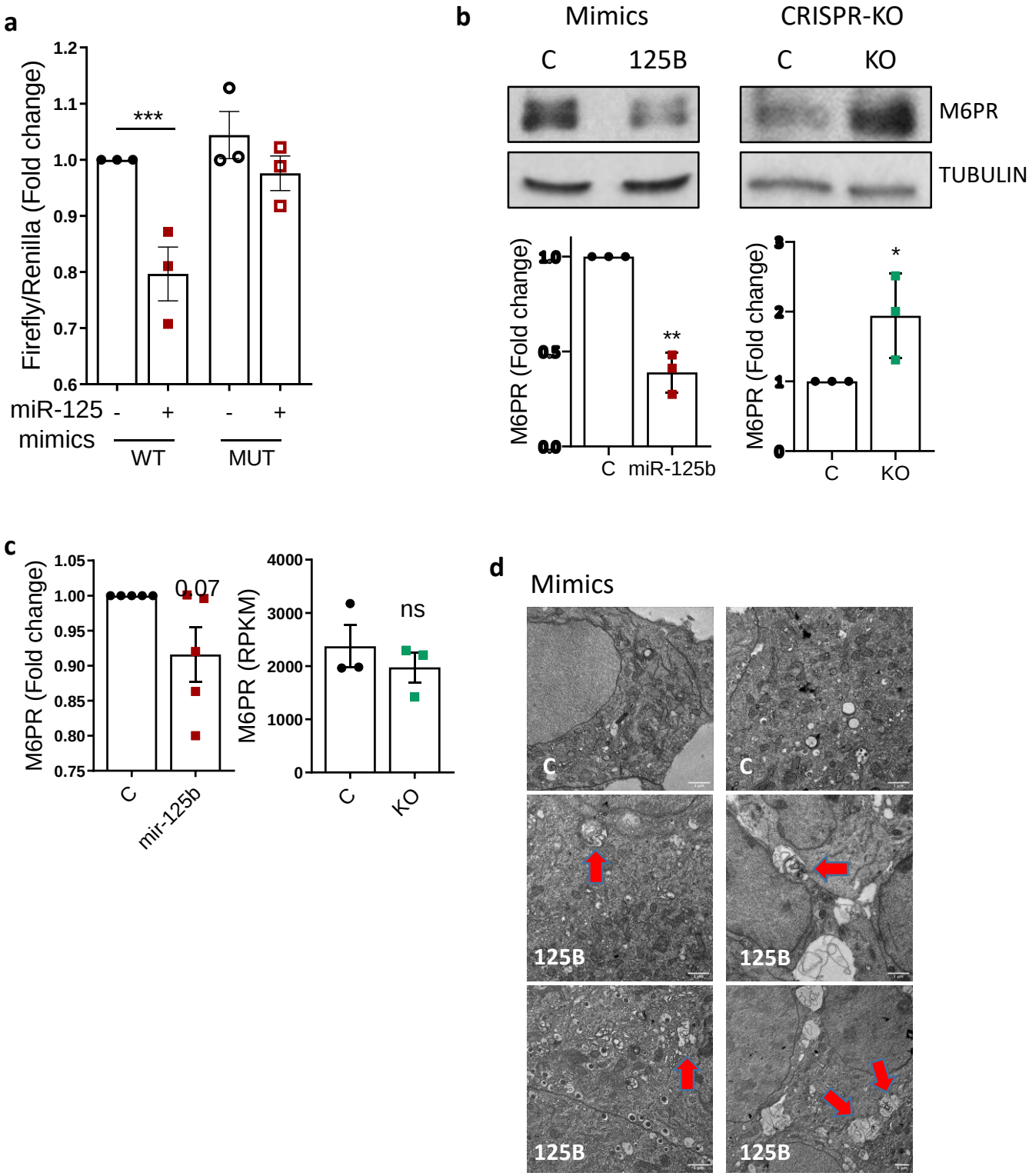
a
Firefly/Renilla (Fold change)
1.2
1.1
1.0
0.9
0.8
0.7
0.6
***
miR-125 mimics
-
+
-
+
WT
MUT
b
Mimics
CRISPR-KO
C
125B
C
KO
M6PR
TUBULIN
M6PR (Fold change)
1.0
0.5
0.0
**
C
miR-125b
3
2
1
0
*
C
KO
c
M6PR (Fold change)
1.05
1.00
0.95
0.90
0.85
0.80
0.75
0.07
C
mir-125b
M6PR (RPKM)
4000
3000
2000
1000
0
ns
C
KO
d
Mimics
C
C
125B
125B
125B
125B

Figure 6

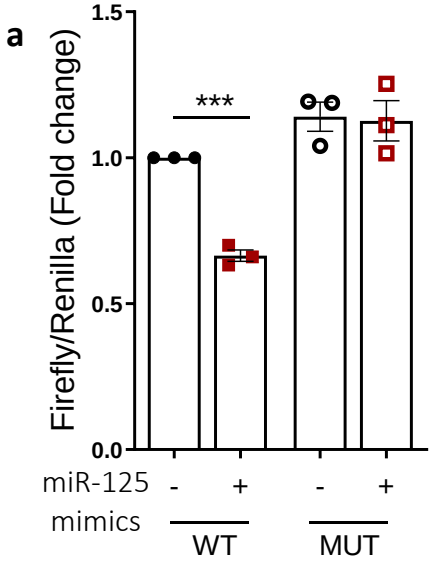
a
Firefly/Renilla (Fold change)
1.5
1.0
0.5
0.0
***
miR-125 mimics
-
+
-
+
WT
MUT

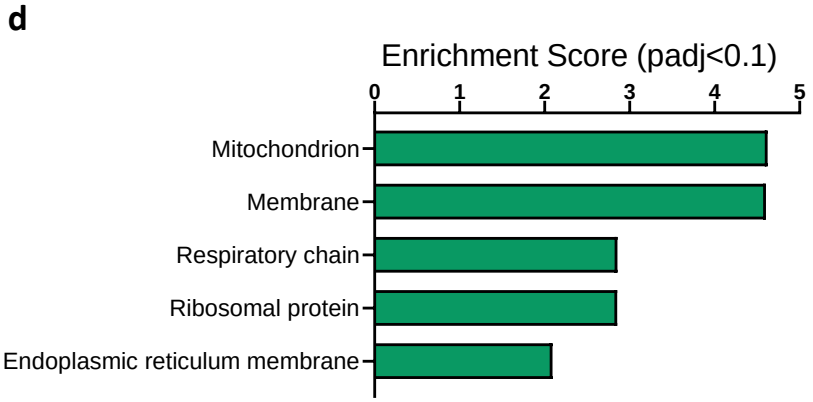
d
Enrichment Score (padj<0.1)
0
1
2
3
4
5
Mitochondrion
Membrane
Respiratory chain
Ribosomal protein
Endoplasmic reticulum membrane

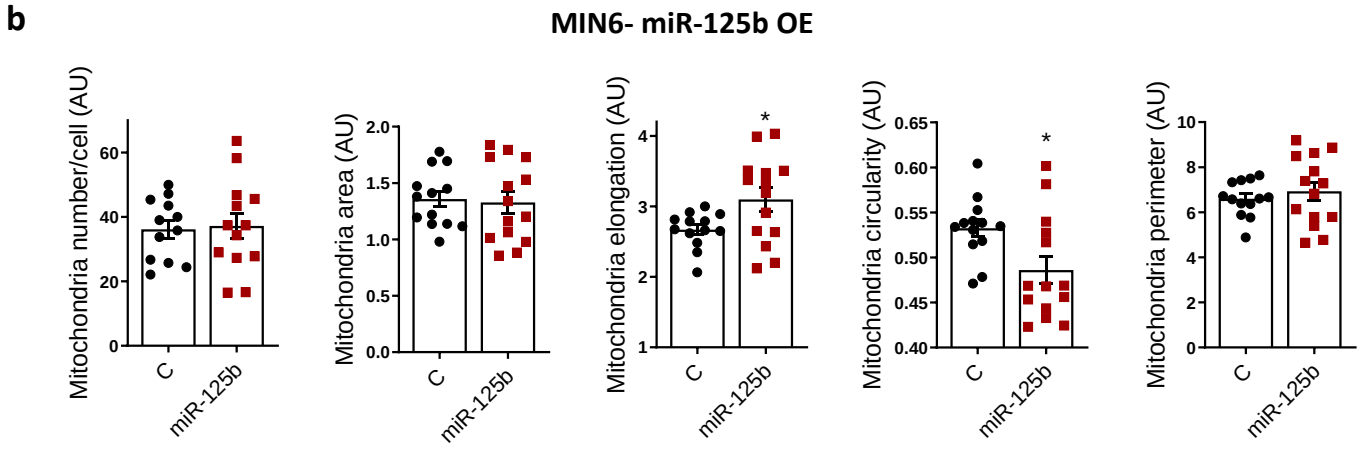
b
MIN6- miR-125b OE
Mitochondria number/cell (AU)
Mitochondria area (AU)
Mitochondria elongation (AU)
Mitochondria circularity (AU)
Mitochondria perimeter (AU)
C
miR-125b
*
*

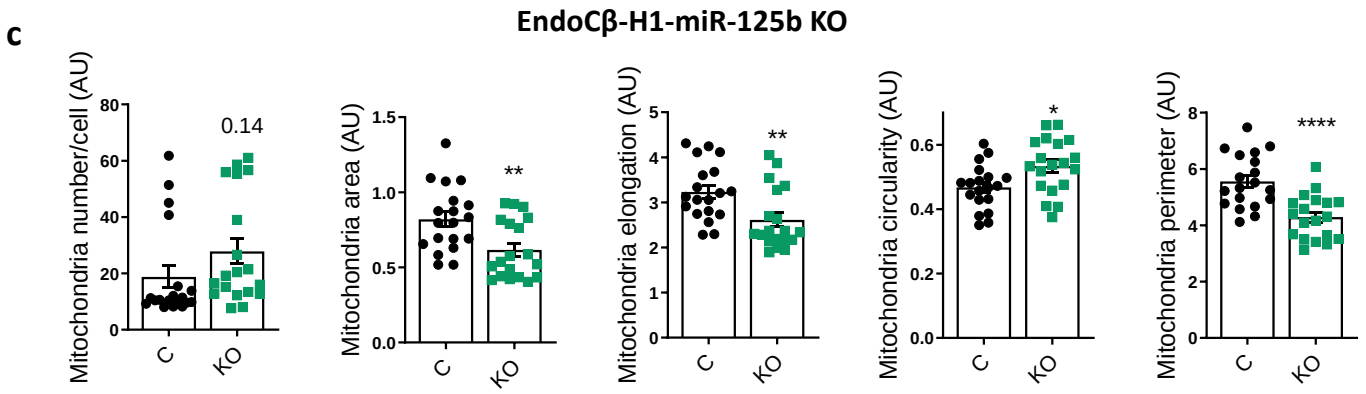
c
EndoCβ-H1-miR-125b KO
Mitochondria number/cell (AU)
Mitochondria area (AU)
Mitochondria elongation (AU)
Mitochondria circularity (AU)
Mitochondria perimeter (AU)
0.14
**
**
*
****
C
KO

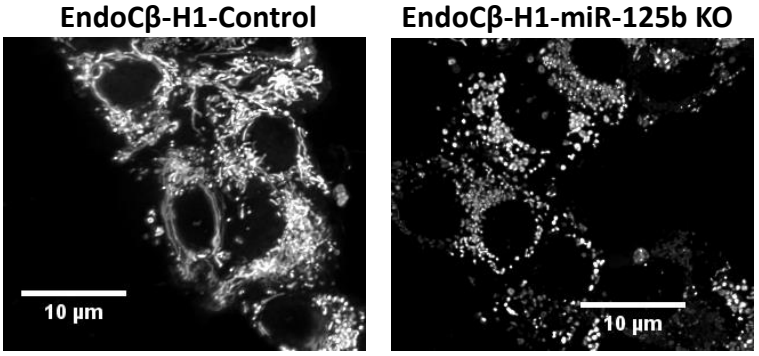
EndoCβ-H1-Control
EndoCβ-H1-miR-125b KO
10 µm
10 µm

Figure 7

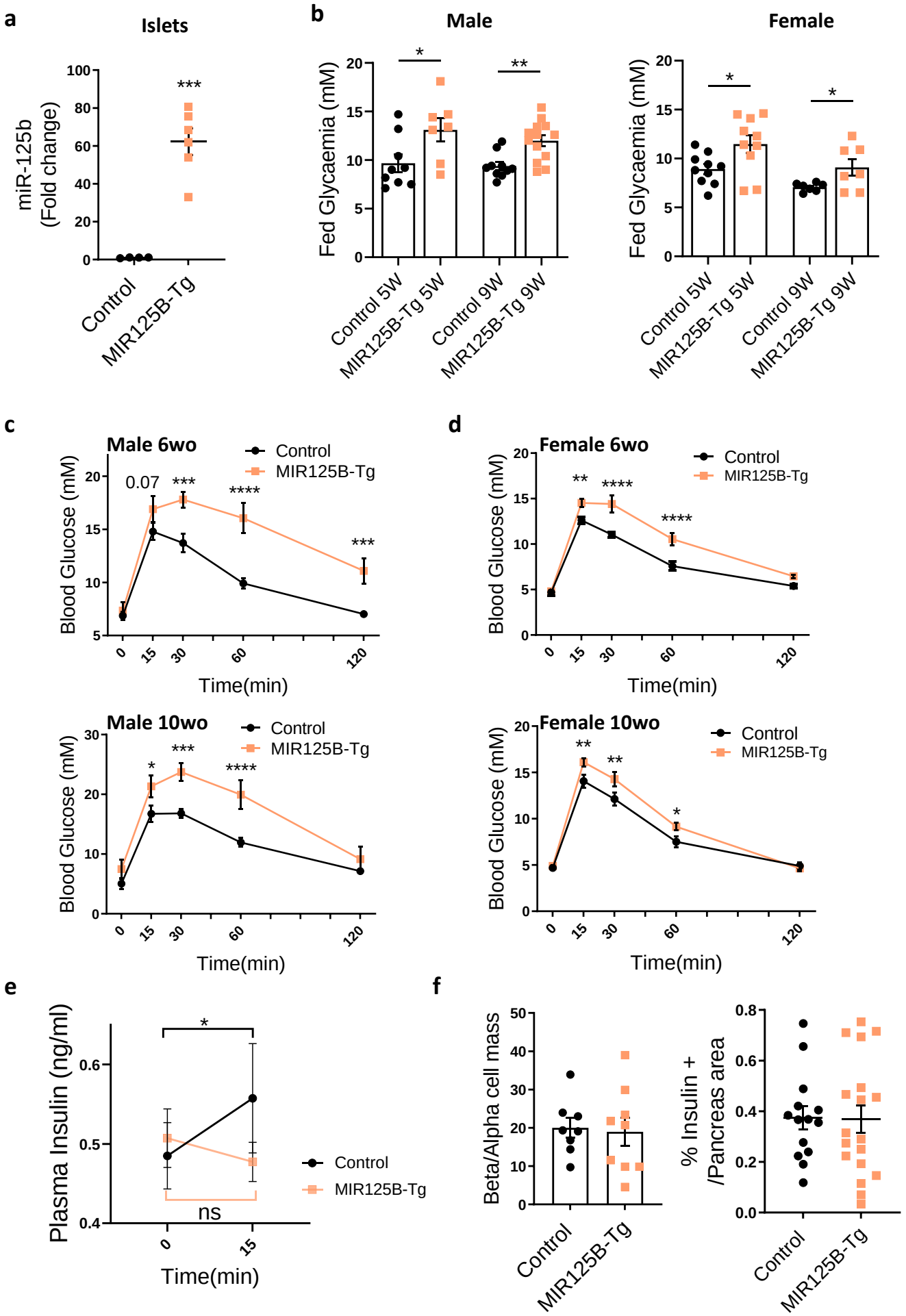
a
Islets
miR-125b (Fold change)
100
80
60
40
20
0
***
Control
MIR125B-Tg
b
Male
Female
Fed Glycaemia (mM)
20
15
10
5
0
*
**
Control 5W
MIR125B-Tg 5W
Control 9W
MIR125B-Tg 9W
c
Male 6wo
Control
MIR125B-Tg
Blood Glucose (mM)
0.07
***
****
Time(min)
0
15
30
60
120
Male 10wo
d
Female 6wo
Female 10wo
e
Plasma Insulin (ng/ml)
0.6
0.5
0.4
ns
f
Beta/Alpha cell mass
50
40
30
20
10
% Insulin + /Pancreas area
0.8
0.6
0.4
0.2
0.0

Figure 8

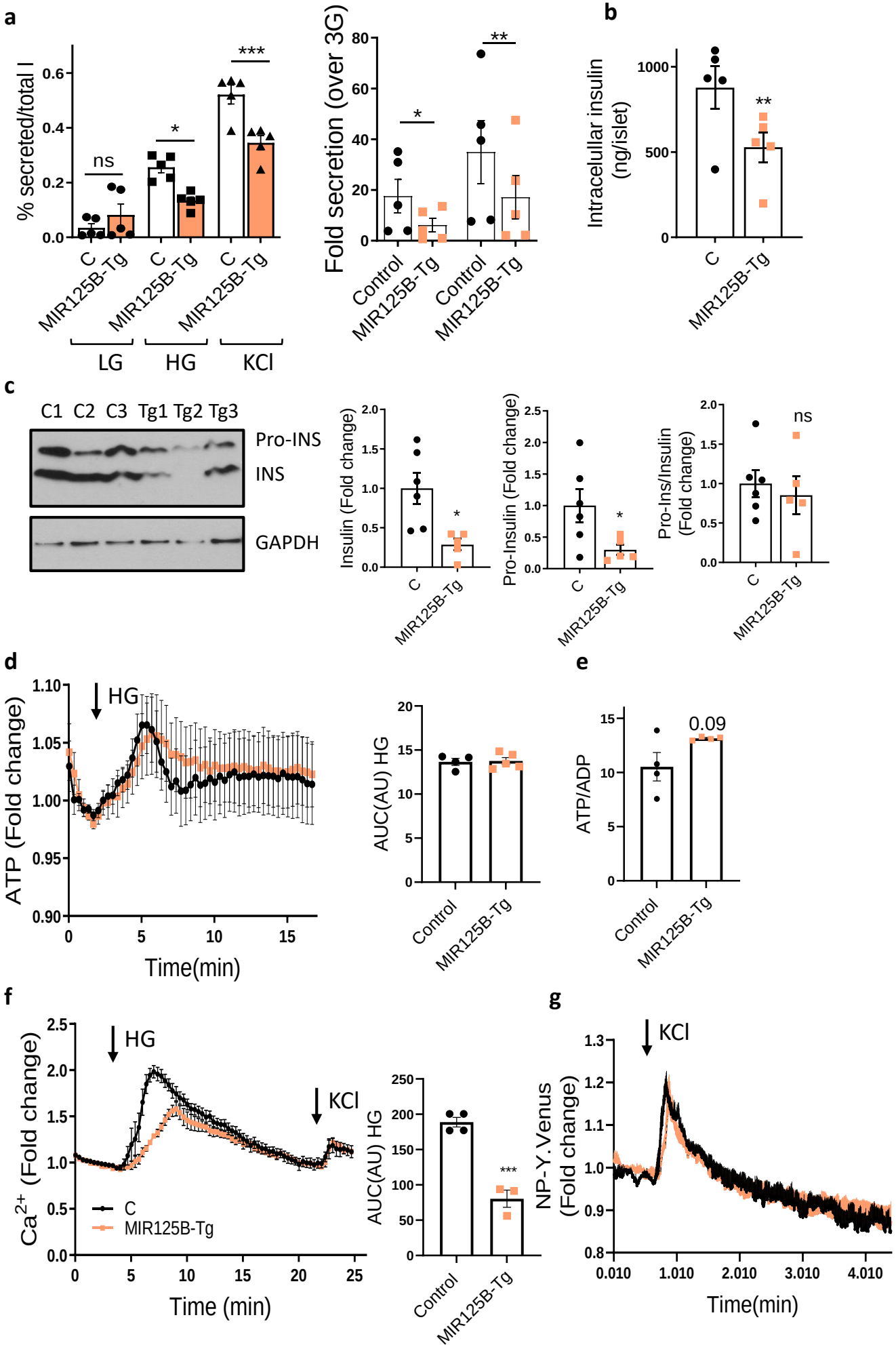
a
% secreted/total I
ns
*
***
C
MIR125B-Tg
LG
HG
KCl
Fold secretion (over 3G)
Control
MIR125B-Tg
b
Intracelullar insulin (ng/islet)
c
C1 C2 C3 Tg1 Tg2 Tg3
Pro-INS
INS
GAPDH
Insulin (Fold change)
Pro-Insulin (Fold change)
Pro-Ins/Insulin (Fold change)
d
HG
ATP (Fold change)
Time(min)
AUC(AU) HG
e
ATP/ADP
0.09
f
KCl
Ca2+ (Fold change)
Time (min)
g
NP-Y.Venus (Fold change)

Figure 9

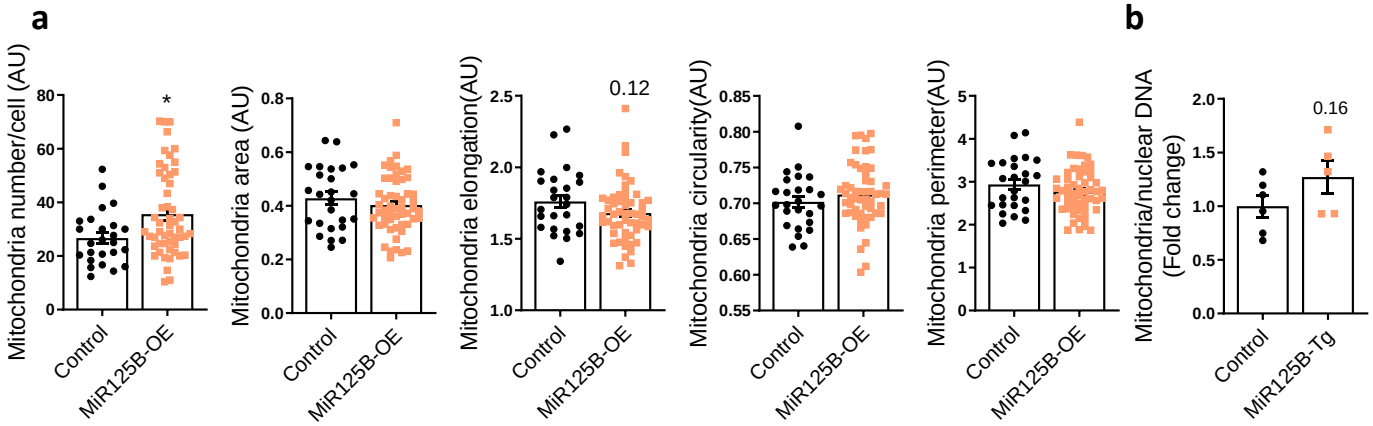
a
Mitochondria number/cell (AU)
Mitochondria area (AU)
Mitochondria elongation(AU)
Mitochondria circularity(AU)
Mitochondria perimeter(AU)
Control
MiR125B-OE
*
0.12
b
Mitochondria/nuclear DNA (Fold change)
0.16
MiR125B-Tg

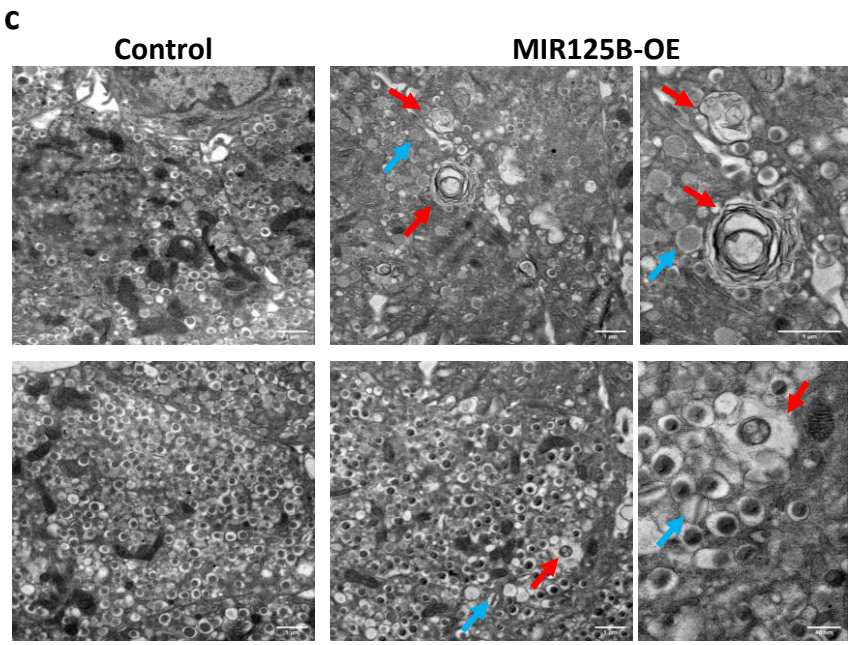
c
Control
MIR125B-OE

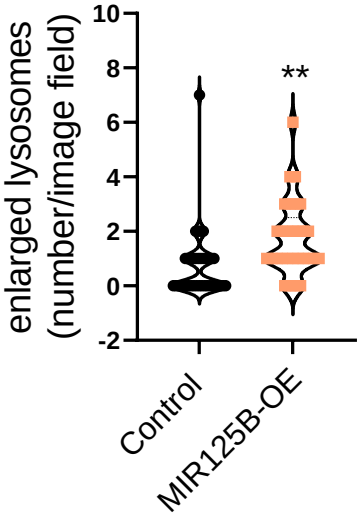
d
enlarged lysosomes (number/image field)
**
Control
MIR125B-OE

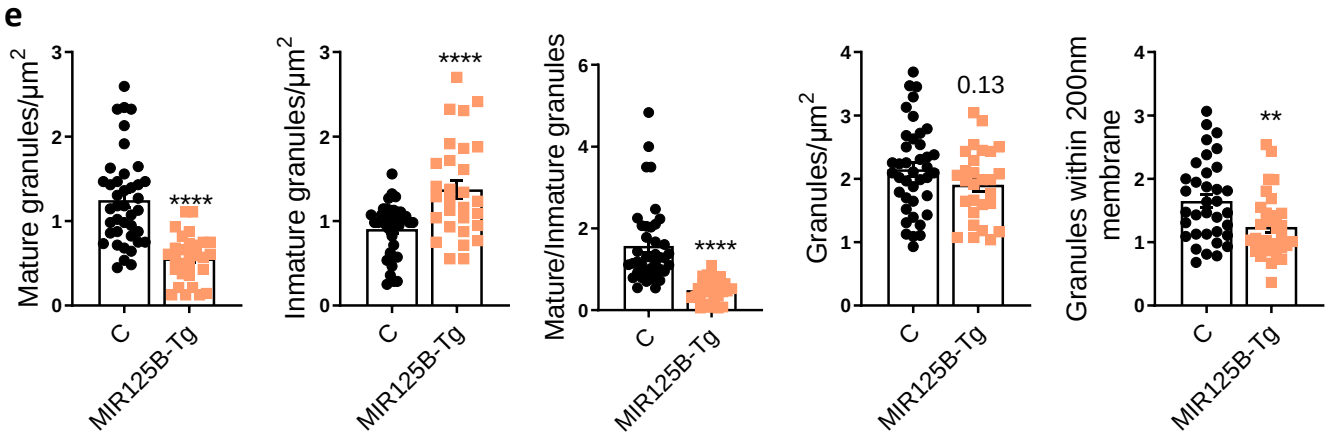
e
Mature granules/μm2
Inmature granules/μm2
Mature/Inmature granules
Granules/μm2
Granules within 200nm membrane
****
0.13
**
C
MIR125B-Tg

Figure 10

a MIR12B-Tg mouse islets- GO/Functional enrichment

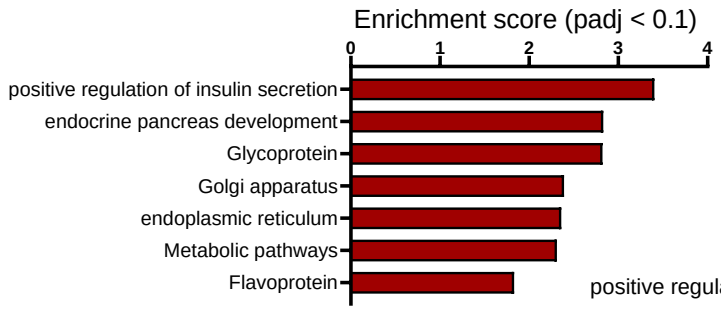

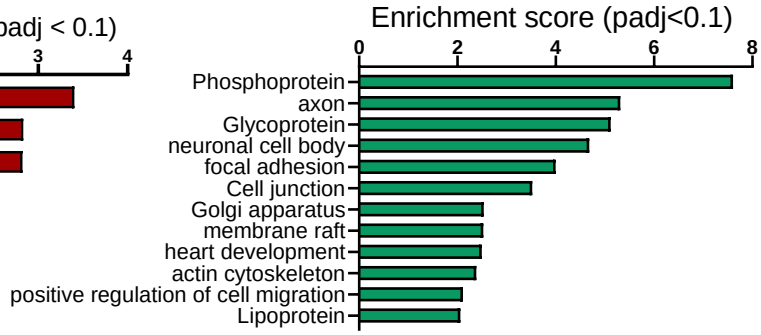

b MIR12B-Tg mouse islets

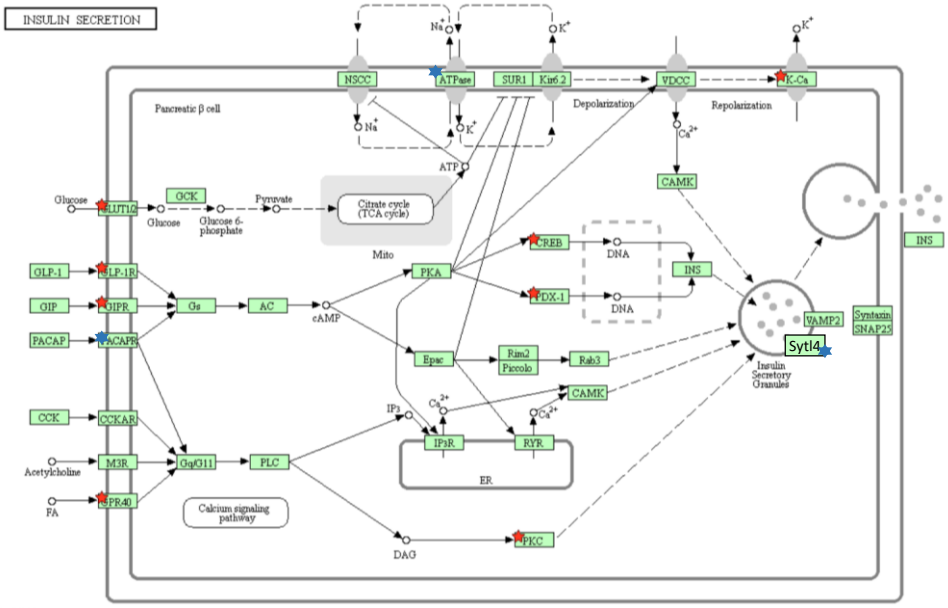

c AD-MIR12B human islets- GSEA

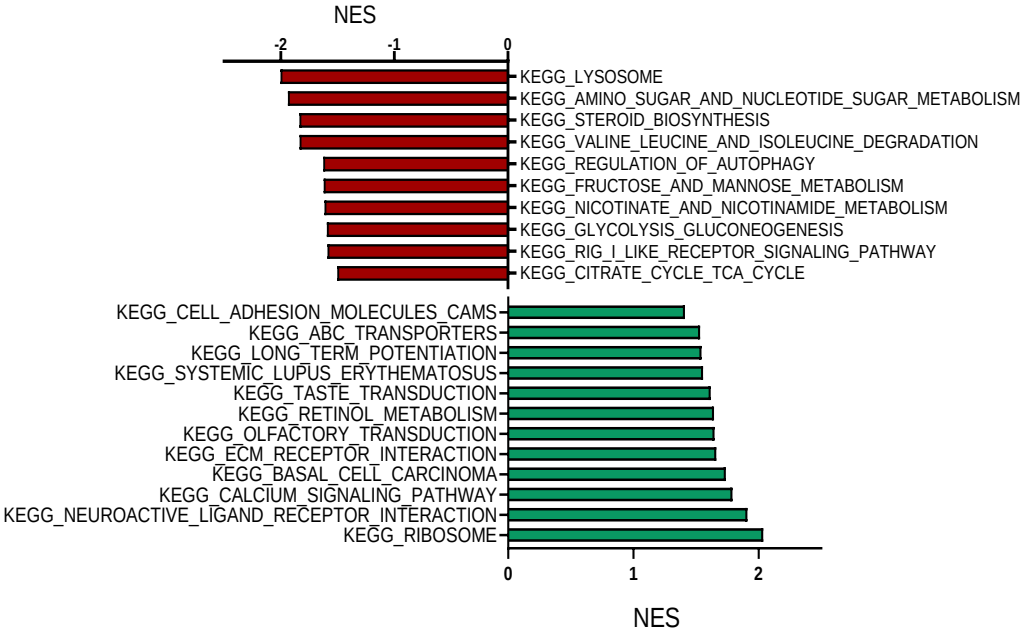

d

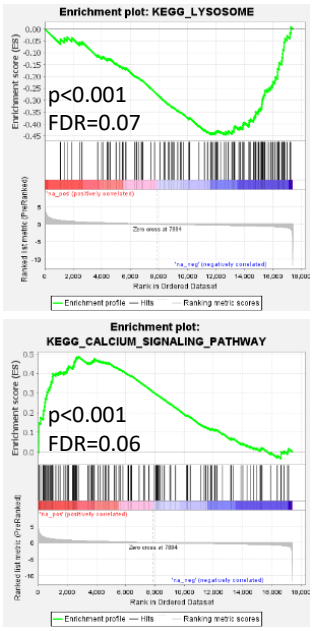

Supplemental Figure 1

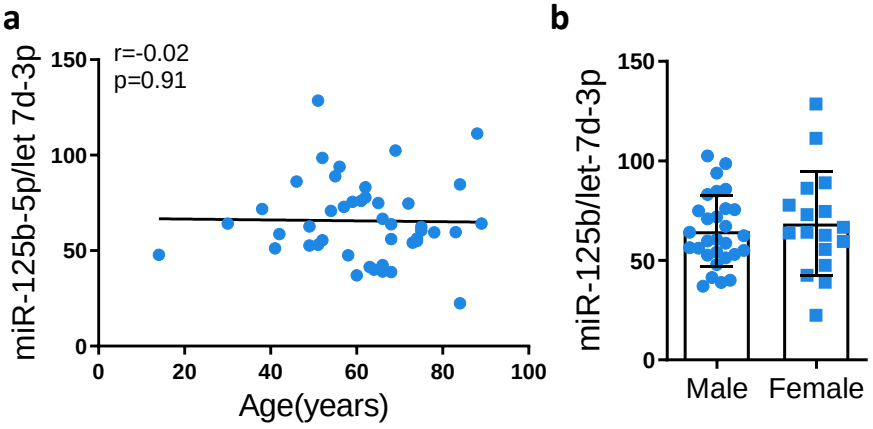

Supplemental Figure 2

a

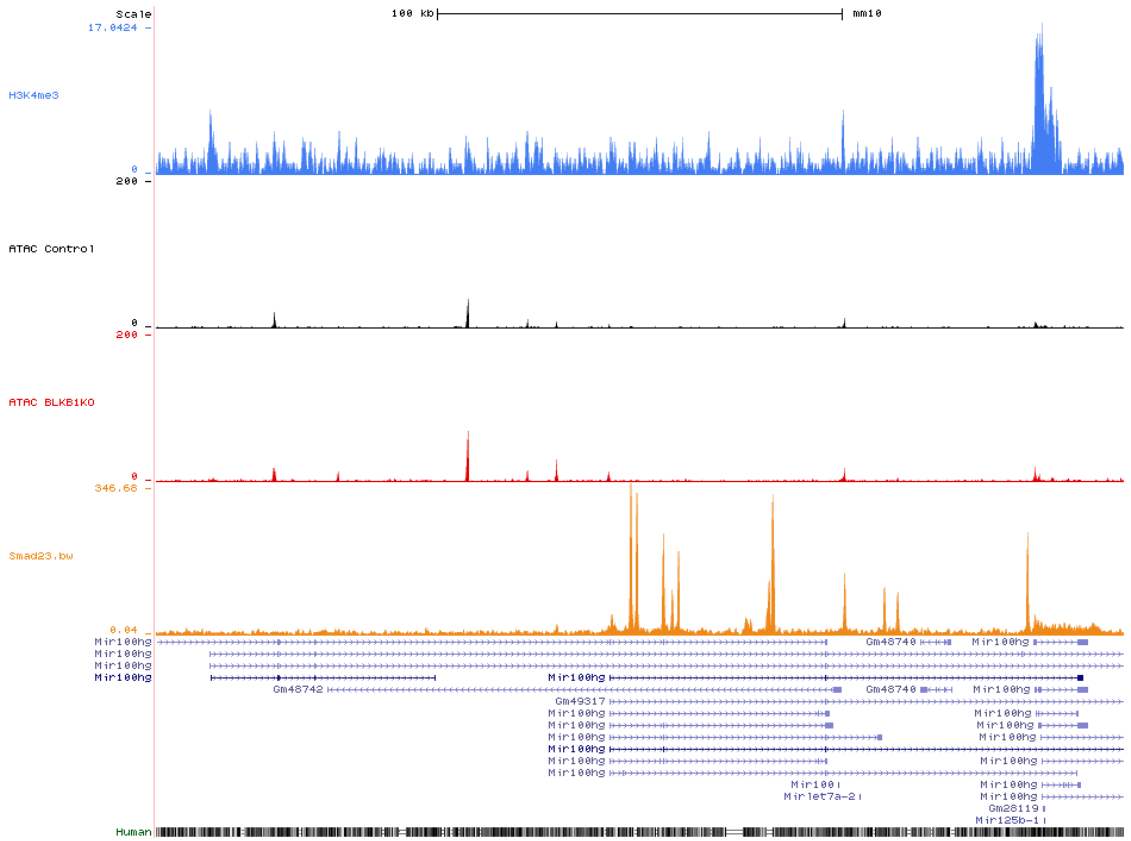

b

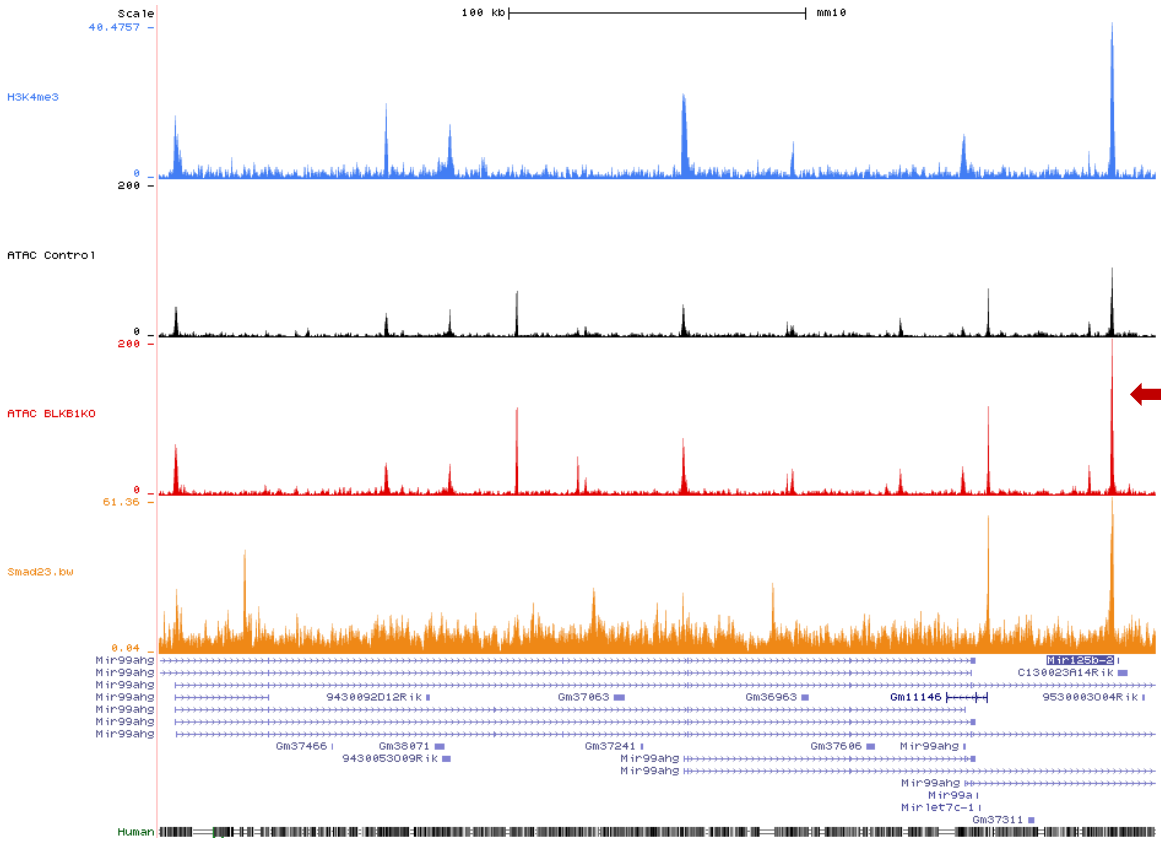

Supplemental Figure 3

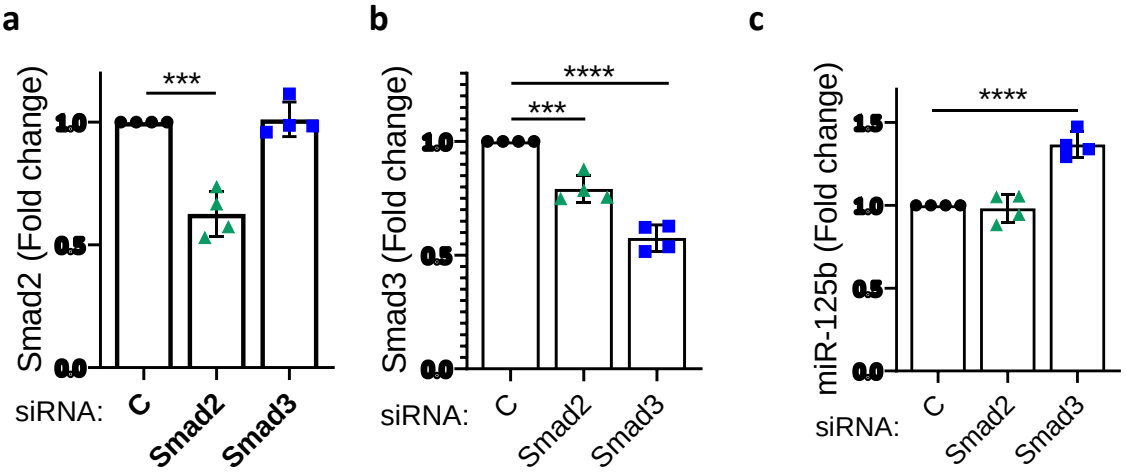

Supplemental Figure 4

a

MIR125B-1

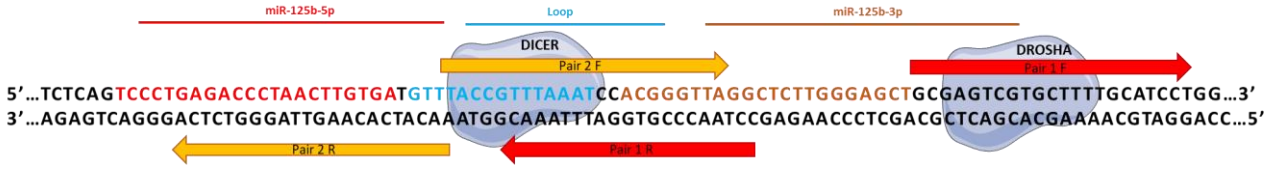

MIR125B-2

b

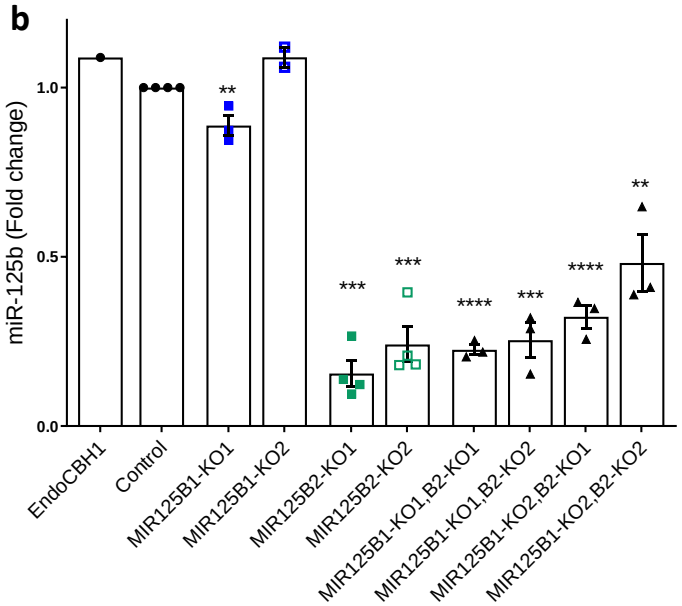

c

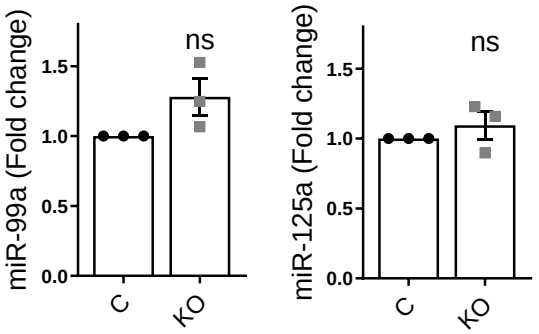

Supplemental Figure 5

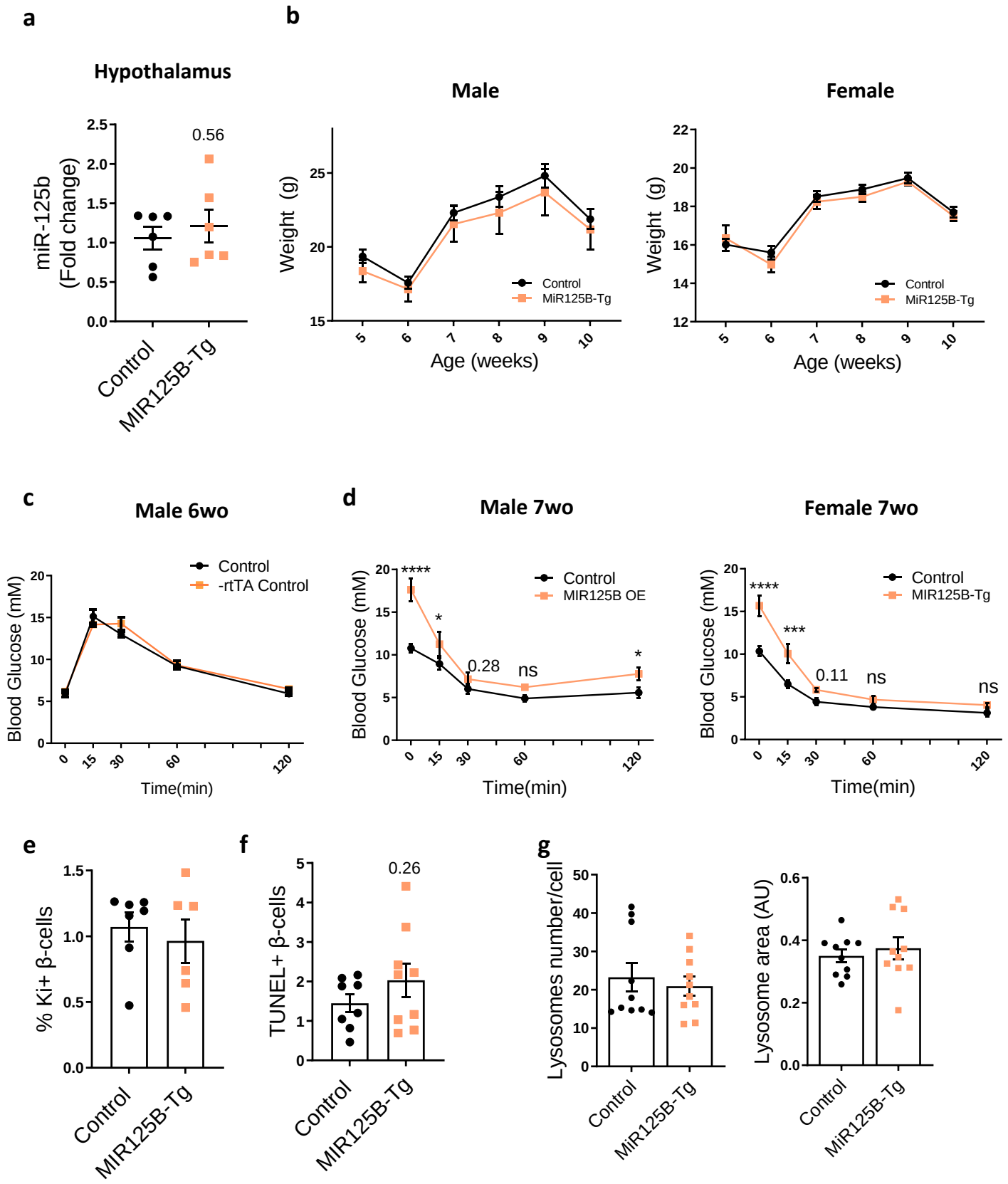
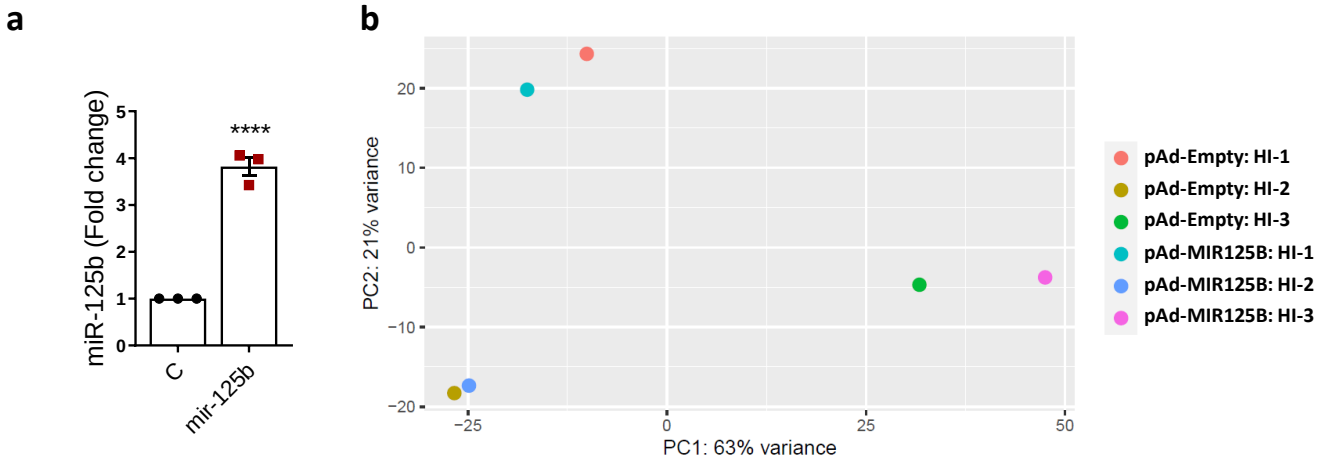
Supplemental Figure 6